Title

Converging Topographic Axes of Connectivity and Genetic Architectures across the Cerebral Cortex

Short title

Cortical Connectopies underpinned by Genetic Gradients

Authors

Deying Li,[1,2] Yufan Wang,[1,2] Liang Ma,[1,2] Weiyang Shi,[1] Yuheng Lu,[1,2] Haiyan Wang,[1] Xinle Cheng,[1,2] Yaping Wang,[1,3] Chaohong Gao,[1,3] Luqi Cheng,[4,5] Camilla T. Erichsen,[6] Yu Zhang,[5] Zhengyi Yang,[1,2,3] Simon B Eickhoff,[7,8] Chi-Hua Chen,[9] Congying Chu,[1*] Lingzhong Fan[1,2,3,10,11*]

Affiliations

[1] Brainnetome Center, Institute of Automation, Chinese Academy of Sciences, 100190, Beijing, China

[2] School of Artificial Intelligence, University of Chinese Academy of Sciences, 100190, Beijing, China.

[3] Sino-Danish College, University of Chinese Academy of Sciences, 100190, Beijing, China.

[4] School of Life and Environmental Sciences, Guilin University of Electronic Technology, Guilin 541004, China.

[5] Research Center for Augmented Intelligence, Zhejiang Lab, 311100, Hangzhou, Zhejiang, China.

[6] Core Center for Molecular Morphology, Section for Stereology and Microscopy, Department of Clinical Medicine, Aarhus University, 8000, Aarhus, Denmark

[7] Institute of Neuroscience and Medicine (INM-7: Brain and Behaviour), Research Centre Jülich, 52425 Jülich, Germany.

[8] Institute of Systems Neuroscience, Heinrich Heine University Düsseldorf, 40225 Düsseldorf, Germany.

[9] Department of Radiology, University of California San Diego, La Jolla, CA 92093.

[10] CAS Center for Excellence in Brain Science and Intelligence Technology, Institute of Automation, Chinese Academy of Sciences, 100190, Beijing, China.

[11] School of Health and Life Sciences, University of Health and Rehabilitation Sciences, 266000, Qingdao, Shandong, China.

[*] Corresponding Author: Lingzhong Fan or Congying Chu, Institute of Automation, Chinese Academy of Sciences, Beijing 100190, China. Phone: 010 – 82544523.

Email: lingzhong.fan@ia.ac.cn or chucongying@gmail.com

Abstract

Genetic factors have involved the gradual emergence of cortical areas since the neural tube begins to form, shaping the heterogenous functions of neural circuits in the human brain. Informed by invasive tract-tracing measurements, the cortex exhibits marked interareal variation in connectivity profiles to reveal the heterogeneity across cortical areas. However, it remains unclear about the organizing principles possibly shared by genetics and cortical wiring to manifest the spatial heterogeneity across the cortex. Instead of considering a complex one-to-one mapping between genetic coding and interareal connectivity, we hypothesized the existence of a more efficient way that the organizing principles are embedded in genetic profiles to underpin the cortical wiring space. Leveraging on the vertex-wise tractography in diffusion-weighted MRI, we derived the global connectopies to reliably index the organizing principles of interareal connectivity

variation in a low-dimensional space, which specifically captured three dominant topographic patterns along the dorsoventral, rostrocaudal, and mediolateral axes of the cortex. More importantly, we demonstrated that the global connectopies converge to the gradients of vertex-by-vertex genetic correlation matrix on the phenotype of cortical morphology and the cortex-wide spatiomolecular gradients. By diving into the genetic profiles, we found the critical role of genes related to brain morphogenesis in scaffolding the global connectopies. Taken together, our findings demonstrated the existence of a genetically determined space to encode the interareal connectivity variation, which may give new insights into the links between cortical connections and arealization.

Teaser

We identify a common space linking genetic profiling and interareal connectivity variation.

MAIN TEXT

Introduction

Mounting evidence has suggested that the genetic effects on the anatomical phenotypes of the human brain are spatially heterogeneous (*1-5*), demonstrating the vital roles of genes in establishing the configuration of brain space, such as the anatomical hierarchy (*6*) and the wiring diagram (*7-9*). Especially the profile of cortical wiring that can be characterized by using neuroimaging-based tractography is a reliable source to indicate the heterogeneity across cortical areas (*10, 11*), reflecting the differentiation in local microstructures and connectivity patterns. The interareal connectivity variation has further revealed the spatially heterogeneous patterns of cortical organization, such as the regional controllability related to cognitive dynamics (*12-14*). In contrast, the deficit of interareal connectivity has demonstrated the specificity to the behavioral manifestations of the brain lesion (*15, 16*). Although the spatial heterogeneity has been separately found to be embedded in genetic architecture and interareal connectivity variation, it is still largely unknown if there exists a unified organizing principle underlying their indication of the spatial heterogeneity.

The spatiotemporal distribution of genetic factors along the developing brain is found to set the primary cues to guide the process of cortical arealization (*17, 18*). It has been pointed out that gene-coded signaling molecules and transcriptional profiles may account for the guidance, which are even conserved to maturity (*19, 20*). Specifically, under the effect of morphogens secreted in the patterning centers, transcription factors are expressed in a graded manner and determine the areal fate and the expression of cell-surface molecules, thus determining the topographic organization of synaptic inputs and outputs (*1, 21*) and directing axonal outgrowth (*22*). Nevertheless, considering the complexity and flexibility of neural circuits, it would be difficult to conceive the existence of a one-to-one mapping between the genetic codes and the wiring patterns (*23*). Alternatively, we hypothesize that the genetic profiles distributed across the cortex may contain the organizing principles of cortical wiring (*23*). In this way, the genetic processes and the cortical wiring patterns can be systematically unified to provide a more complete understanding of the heterogeneity across the cortex. Recent advances in acquiring high-throughput transcriptomic data of the human brain (*24*) and large-scale twin samples (*2, 3*) with neuroimaging data provide essential resources to test our hypothesis.

Furthermore, even if we could identify the genetic topography accounting for the cortical heterogeneity, we would still need to verify whether we could leverage it to unify the interareal connectivity variation captured by high-resolution connectomics (*25, 26*). Recent studies revealed that cortical areas are hierarchically along the cortex from a large-scale gradient perspective of connectivity (*27, 28*), indicating that the cortex is organized topologically within interareal connectivity variation, supporting diverse dynamics and functions (*29-32*). However, traditional

neural circuit tracing techniques, including classical tracers or virus tracing, are precluded in humans, thereby creating the need for noninvasive measures of the topography embedded in interareal connectivity variation, which would contribute to testing the existence of unified rules underlying the genetic topography and interareal connectivity variation.

Therefore, we combined diffusion tractography with a dimension reduction framework and revealed three modes of fine-grained white-matter organization, i.e., global connectopies. The three global connectopies run separately along the dorsoventral, rostrocaudal, and mediolateral axes, formed by gradual shifts in connectivity driven by specific scaffolding white matter tracts, which we mapped to distinct modes of function. Similar to the first axis, the other two connectivity axes were not constrained *a priori* to follow any spatial organization of the brain (e.g., spatial coordinates, cytoarchitecture, or macroscale anatomy) but instead were allowed to reveal how the anatomical and axial alignments are embedded in the intrinsic structure of transcriptional variation. We then explored how the three axes are biologically and developmentally distinct and demonstrated that they constrained the cortical patterning to a certain extent and could be used to explain most of the spatial variation across key anatomical and functional brain maps derived from neuroimaging. Moreover, we demonstrated a correspondence between the genetic influence on cortical morphology and the global connectopies and identified genes associated with the global connectopies that are also involved with brain morphogenesis. We further established that the three global connectopies are consistent with morphogen gradients in the developing brain and spatiomolecular gradients in adulthood and provided evidence that specific genes drive the formation of the cortical organization. The current study highlights the genetic origin of structural connections as the foundation of brain function and provides essential insights into the topographic principles of brain organization.

Results

Three global connectopies in the human brain

To explore how the spatial organization of the human brain is shaped by the underlying structural connections with the white matter, we characterized the global connectopies across the whole brain (Figure 1a, left). We first built a vertex-wise structural connectivity similarity profile matrix using 100 unrelated subjects from the Human Connectome Project dataset (*33*). Specifically, structural connectivity profiles were obtained from probabilistic tractography along ~30k vertices for each hemisphere and were correlated between each pair of vertices. Tractogram covariance (TC) matrices were thresholded at 0 and averaged across subjects. In short, the TC matrix captured structural connectivity similarity across the whole brain.

We implemented diffusion embedding on the TC matrix, a manifold learning method previously used to capture functional gradients (*34*). The resultant components revealed the position of vertices along the axes that had the most dominant differences in the given structural connectivity profile. The first three global connectopies separately showed dorsoventral, rostrocaudal, and mediolateral patterns (Figure 1b) and together accounted for 33% of the total variance (Figure 1a, right).

More specifically, the first global connectopy (Global connectopy 1 dorsoventral, GC1-DV), following a dorsoventral pattern, was anchored on one end by the occipital, inferior temporal, and orbital frontal cortex and on the other end by the motor and sensorimotor cortex. The second global connectopy (Global connectopy 2 rostrocaudal, GC2-RC) varied along a rostrocaudal axis, radiating from the occipitoparietal cortex and ending in the prefrontal cortex. The third global connectopy (Global connectopy 3 mediolateral, GC3-ML) showed a mediolateral pattern, with the highest expression in the lateral temporal and prefrontal cortex and the lowest in the cingulate cortex (Figure 1b).

These patterns were stable regardless of the number of subjects considered (Figure S1) and were not affected by age, sex, or brain size (Figure S2). Individual GCs were computed for each

subject and aligned to the group GC with Procrustes rotation, allowing for comparison between individuals. The individual global connectopies highly correlated with the group GC (all $r > 0.9$; Figure S3). We further showed that global connectopies are beyond geodesic distance (Figure S4) and demonstrated the role of long-range connections in the formation of global connectopies (Figure S5).

To investigate whether these global connectopies recapitulated the biological basis of the brain organization, we mapped the distribution of these global connectopies according to their laminar differentiation (*35*) and cytoarchitecture classes (*36*). The idiotypic regions identified by laminar differentiation revealed two extremes in the GC1-DV, with the dorsal end corresponding to the primary second sensory cortices in terms of cytoarchitecture classification and the ventral end affiliated with the primary motor network (Figure S6, 7) and corresponding to the visual network and sensorimotor network in terms of Yeo's intrinsic functional network (*37*). Most of the idiotypic regions and the areas of unimodal cortex were located in the posterior extreme of the GC2-RC, and the cingulate cortex, part of the limbic network, varied broadly along the global connectopy by the "anterior-posterior" pattern of the global connectopy (Figure S6). The medial part of the GC3-ML occupied the paralimbic cortex, while the lateral part was primarily situated in the association cortex, or heteromodal cortex (Figure S7). These differences demonstrated the cytoarchitectural distinctiveness in the regions at the extremes of the global connectopies.

Note that different regions along the global connectopies belong to distinct intrinsic functional networks. We thought that these affiliations might involve different cognitive functions, so we conducted a meta-analysis to investigate this relationship. The ventral end of GC1-DV was characterized by a visual network that includes "navigation," "episodic," and "faces." In contrast, the dorsal end is characterized by terms about sense and movement, such as "limb," "foot," and "finger" (Figure 1c, left). In GC2-RC, we observed a focus on multisensory and motion terms anteriorly and on "tactile" and "finger" processing posteriorly (Figure 1c, middle). GC3-ML was related to "autobiographical," "craving," and "gestures" in medial regions and to "competing," "risking," and "sentences" in lateral regions (Figure 1c, right).

We also collected a selection of brain maps from neuromaps (*38*) and other public studies (*39*) and made a comparison with the global connectopies (Figure S8, 9). We found that GC1-DV was correlated with the second functional gradient captured by functional connectivity ($r = -0.64$, $p_{spin} < .0001$), which differentiates regions within the unimodal cortex, whereas GC2-RC showed correlation with the first functional gradient ($r = -0.49$, $p_{spin} < .0001$). Notably, the global connectopies showed high correlations with MEG recording maps, including the alpha, beta, delta, gamma, and theta bands ($r_{GC1\text{-}DV,\ beta} = 0.91$, $r_{GC1\text{-}DV,\ theta} = 0.62$, $r_{GC2\text{-}RC,\ delta} = -0.64$, $r_{GC2\text{-}RC,\ gamma1} = -0.62$, $r_{GC2\text{-}RC,\ gamma2} = -0.52$, $r_{GC2\text{-}RC,\ theta} = -0.51$, all $p_{spin} < .0001$, Figure S8, 9). These results support the view that the underlying brain structure is fundamental to the functions across the brain, providing insights into the relationship between microscale structural and macroscale functional features of the cortex.

The three connectopies are situated by distinct sets of white matter tracts

We further explored how the underlying white matter shaped these spatial organizations. We fitted general linear models (GLMs) to interpolate measures from the gray matter into the white matter (*40*). Specifically, we used the global connectopies as a dependent variable and the structural connection matrix as an independent variable, thus projecting each global connectopy onto the white matter (Figure S10). For GC1-DV, the white matter voxels were distributed along the ventral-dorsal axis beneath the surface. Specifically, voxels lying near the sensorimotor/motor cortex and occipitotemporal cortex showed values that were markedly consistent with the locations of the extremes of the first global connectopy. Voxels corresponding to GC2-RC and GC3-ML varied from posterior to anterior and medial to lateral.

Since the white matter is mainly composed of tracts, we then focused on the specific tracts related to the emergence of the global connectopies. We reconstructed 72 fiber bundles following

TractSeg (*41*) (Table S1) and built group-level connectivity blueprints (*42*). Figure S11c shows the distribution of the blueprint along the global connectopies. We also generated global connectopies based on the connectivity blueprint following the same procedure (Figure S11a). Specifically, we built a TC matrix by correlating pairs of vertices from the connectivity blueprint and also used diffusion map embedding. The global connectopies generated by the blueprints were very similar to the results calculated by the original structural connection (Figure 1b, Figure S11a; left: $r_{\text{GC1-DV}} = 0.91$, $r_{\text{GC2-RC}} = 0.86$, $r_{\text{GC3-ML}} = 0.65$; right: $r_{\text{GC1-DV}} = 0.94$, $r_{\text{GC2-RC}} = 0.82$, $r_{\text{GC3-ML}} = 0.53$), indicating that low-dimensional connectivity blueprints could provide a descriptor of the structural connectivity information in the brain.

We then produced tract projection maps using the connectivity blueprints. We first extracted the projection on the surface of each tract and calculated the mean value and variance of connectopy values of tract projection on the surface (Figure 2). We identified the tracts that were either situated at one of the extremes of the global connectopy or were spread out along the axis. The results for the bilateral tracts were averaged between the two hemispheres and are shown in the scatterplot (Figure 2, detailed values are shown in Figure S12).

Two types of characteristic tracts are shown in the right columns of Figure 1c, including T_PREC, ST_OCC, and T_PAR for GC1-DV as well as MLF, T_PREF, SLF_II for GC2-RC along with AF, CG, and MLF for GC3-ML.

For GC1-DV, the thalamo-precentral tract (T_PREC), which connects the thalamus with the precentral gyrus, is related to motor task performance (*43, 44*). T_PREC has a distinctly vertical expanding shape and showed high mean values near the dorsal end of GC1-DV, thus expressing the most significant contribution to the global connectopy. The striato-occipital (ST_OCC) tract connects the striatum with the occipital cortex, showing high mean values at the ventral end and having a “stretching” impact on the global connectopy pattern. In contrast, the thalamo-parietal tract (T_PAR) has a high variance within the GC1-DV and appears to constrain the global connectopy formation.

For GC2-FC, the second branch of the superior longitudinal fascicle (SLF_II), which mostly runs from the posterior to the anterior, starting from the middle frontal gyrus and terminating in the angular gyrus, had the greatest mean value for the white matter tract. The SLF_II, which covered most of the areas in the second global connectopy, also showed high values, providing the prefrontal cortex with parietal cortex information about the perception of visual space and providing information about working memory in the prefrontal cortex to the parietal cortex to focus spatial attention and regulate the selection of spatial information (*45, 46*). Other “high-contribution” tracts, including the MLF and T_PREF, are either in the anterior or posterior regions.

The GC3-ML showed a similar pattern to the tracts that made high contributions. The corpus callosum, the giant white matter fiber bundle consisting of millions of axonal projections, spans from the medial brain through the different parts of the cortex and connects all the brain lobes. Thalamo- and striato-cortical projections also project from the subcortical nuclei and reach the different lateral cortices. We suggest that the former type of tract plays a role in stretching the brain along the axis while the latter type has a constraining effect and that these two work together to shape the organization of the brain.

Global connectopies provide a large-scale descriptor of arealization

To inspect the global connectopies as a unit, we normalized three connectopy values at each vertex to generate RGB values and mapped them on the surface to make lobes or subregions seen distinctly (Figure 3a). We termed this map, the global connectopic space, which quantified the topography of the dominant global connectopy. The cortex, shown in red, green, and blue, indicated the individual regions that were dominated by each global connectopy. The regions that were dominated by a combination of more than one global connectopy were done in different

colors, e.g., the "yellow" region was dominated by the first and second global connectopies together, as shown in the cube in Figure 3a.

We then plotted every pair of global connectopies in a 2D space and assigned colors based on the global connectopic space in Figure 3a. The first and the second global connectopies interacted to split the whole brain into the prefrontal cortex and limbic cortex, sensorimotor and motor cortex, and occipitotemporal cortex (Figure 3b). Similarly, the frontal cortex, limbic cortex, and occipitotemporal cortex were shown when the first and the third global connectopies were considered together, and the prefrontal cortex, limbic cortex (Figure 3b), and others were shown when the second and the third connectopy were combined (Figure 3b). The three GCs were also plotted together in the 3D space. Vertices were assigned different colors according to the signs of the three axes (Figure 3b, right).

In order to show the modules clearly in the global connectopic space, we also partitioned the brain by hierarchical clustering using the three global connectopies (Figure 3c). At the first level, the brain was partitioned into two modules based on the positive and negative signs of the first global connectopy. These two modules coincided with the division between the dorsal and ventral brain regions. Each module was further partitioned into two modules at each level by the sign of the global connectopies. The rostrocaudal and mediolateral patterns emerged after the corresponding global connectopy was considered. In the end, eight modules were captured. These were the ventral and dorsal somatomotor cortex, lateral prefrontal cortex, cingulate gyrus, lateral temporal cortex + angular gyrus, medial occipital cortex + occipital polar cortex, orbitofrontal cortex, and ventromedial prefrontal cortex + posterior cingulate cortex (Figure 3c).

We found that both the four-module and eight-module divisions showed overlap with one of the classes of laminar (Figure S13a and S14a), cytoarchitecture (Figure S13b and S14b), consistent with brain areas defined by histology or a hereditary pattern, suggesting that the global connectopies provided a large-scale descriptor of the structural connectivity and the arealization of the brain.

Potential genetic basis underlying global connectopies

Having established the global connectopies in the human brain, we first explored the relationship between the genetic influence on cortical morphology with the identified global connectopies. We replicated the global connectopies using twin data from the HCP, and found they show high similarity with the results derived from unrelated subjects (left: $r_{\text{G1-DV}} = 0.99$, $r_{\text{G2-RC}} = 0.99$, $r_{\text{G3-ML}} = 0.99$; right: $r_{\text{G1-DV}} = 0.99$, $r_{\text{G2-RC}} = 0.98$, $r_{\text{G3-ML}} = 0.98$; Figure S15). We estimated the pairwise genetic correlation between vertices on the cortex, which revealed shared genetic influences on cortical thickness and relative area expansion between cortical vertices. The first three gradients decomposed from the genetic correlation matrix of cortical thickness showed a rostral-caudal axis, a medial-lateral axis, and a dorsal-ventral axis (left: $r_{\text{GC1-DV, GG3-Thickness}} = 0.72$, $p_{\text{spin}} < .0028$, FDR corrected; $r_{\text{GC2-RC, GG1-Thickness}} = 0.91$, $p_{\text{spin}} < .0001$, FDR corrected; $r_{\text{GC3-ML, GG2-Thickness}} = 0.72$, $p_{\text{spin}} < .0041$, FDR corrected; right: $r_{\text{GC1-DV, GG3-Thickness}} = 0.73$, $p_{\text{spin}} < .0044$, FDR corrected; $r_{\text{GC2-RC, GG1-Thickness}} = 0.88$, $p_{\text{spin}} < .0098$, FDR corrected; $r_{\text{GC3-ML, GG2-Thickness}} = 0.71$, $p_{\text{spin}} < .1566$, FDR corrected; Figure 4a, 4b). The first three gradients decomposed from the genetic correlation matrix of the surface area correspond with the three global connectopies (left: $r_{\text{GC1-DV, GG1-Area}} = 0.53$, $p_{\text{spin}} < .1630$; $r_{\text{GC2-RC, GG2- Area}} = 0.49$, $p_{\text{spin}} < .0006$, FDR corrected; $r_{\text{GC3-ML, GG3- Area}} = 0.51$, $p_{\text{spin}} < .1031$; right: $r_{\text{GC1-DV, GG1-Area}} = 0.58$, $p_{\text{spin}} < .2131$; $r_{\text{GC2-RC, GG2- Area}} = 0.46$, $p_{\text{spin}} < .0177$; $r_{\text{GC3-ML, GG3- Area}} = 0.51$, $p_{\text{spin}} < .0812$; Figure S16). Each parcel derived by the fuzzy clustering of the genetic correlation matrix of cortical thickness (*2*) also showed significant overlap with one of the four parcels derived from the hierarchical clustering identified using the global connectopies (Figure 4c, Figure S13c, d and Figure S14c, d). Overlap between parcels derived from the hierarchical clustering and parcels from the genetic correlation of surface area were additionally shown in Figure S13e, f and Figure S14e, f. These significant correspondence levels indicated a close genetic relatedness of the global connectopies.

We next explored the roles of the genes that contributed to the global connectopies. Here we focused on the genes in the top 5% of each global connectopy (corrected for multiple comparisons). We found that a selection of genes contributed to more than one global connectopy, with 22 genes overlapping with all three (Figure 5a right). Gene enrichment analyses using different gene sets showed that genes that contributed to only one global connectopy, especially GC2-RC, were involved with biological processes (Figure 5c). The top genes in each global connectopy, such as *FARSA*, *MPND*, *SYCP2*, *CUX1*, *ARHGDIG*, and *NUDT14*, are known to be associated with the regulation of transcription factor activity, morphogenesis, cell proliferation, and metabolic processes (Figure 5b) (*47-53*). Genes related to all three global connectopies showed an obvious connection with various diseases (Figure 5c), with the top genes including *ADAMTSL1* and *TIAM1*, whose mutations can cause several diseases (Figure 5b) (*54-56*). Digging deeper into specific biological processes, we found an enrichment of terms related to the regulation of transcription, metabolic process, morphogenesis, cellular development, and neuron projection (Figure 5d).

Exploring the developmental pattern of the genes associated with global connectopies, we found that these genes were expressed highly in the prenatal period in all lobes and that their expression decreased after birth (Figure 5e), suggesting that the patterns present in adulthood were nearly reached in the early stages of development.

Since the morphogen gradients have been established and their pattern was conserved during the development (*20*), we explored whether these genetic patterns correspond with those of the structural connectivity. We first identified the genes in AHBA that are strongly expressed in one end of the brain, according to a previous publication (*57*). 18 of these genes overlapped with the genes identified to contribute to three global connectopies (hypergeometric test, $p < .001$; Figure 5b). Then we subdivided the connectopies equally into ten parts. Two sample t-tests was used to assess the difference of gene expression of these genes between the first and the last bin. We found expression of *FGF17* was significantly higher in the dorsal cluster than the ventral cluster ($t = 27$, $p < .001$), while the expression of *FOXG1* was significantly higher in the ventral ($t = -25$, $p < .001$). The same opposite patterns were observed between *FGF8* (rostral < caudal, $t = -33$, $p < .001$) and *PAX6* (rostral > caudal, $t = 29$, $p < .001$), and *SFRP1* (medial < lateral, $t = -41$, $p < .001$) and *WNT3* (medial > lateral, $t = 99$, $p < .001$) (Figure 6a). The number of subdivisions does not affect the final results (Figure S17).

We also showed that the three global connectopies showed significant correlations with the spatiomolecular gradients (*20*) ($r_{\text{GC1-DV, LV1}} = 0.74$, $p_{\text{spin}} < .0060$, FDR corrected; $r_{\text{GC2-RC, LV2}} = 0.75$, $p_{\text{spin}} < .0012$, FDR corrected; $r_{\text{GC3-ML, LV3}} = 0.5$, $p_{\text{spin}} < .0233$, FDR corrected; Figure 6b). The spatiomolecular gradients were reported to remain the same pattern as morphogenetic gradients during development. Note that the gradient values for the subcortex, cerebellum, and brainstem were excluded, and only data for the cortex were considered. Since the LV3 gradient showed the most variation and varied along a mediolateral and dorsoventral direction, as mentioned in (*20*), the *r*-value was lower compared with the former two but still significant, and the correlation between the first global connectopy was also moderate ($r_{\text{GC1-DV, LV3}} = -0.36$, $p_{\text{spin}} < .05$). These again suggested a potential genetic basis underlying the global connectopies.

Discussion

In the current study, we demonstrated that a low-dimensional, topological representation of brain connectivity exists and may share common space with gene expression, despite the significant disparity in the numbers of genes and connections. We systematically analyzed the spatial topography of cerebral connectivity, i.e., the white matter tractogram, and identified three orthogonal global connectopies: the dorsoventral, rostrocaudal, and mediolateral connectopy across the cerebral cortex, which is represented in the spatial arrangement of long-range white matter tracts. Moreover, the global connectopies were observed to be aligned with the gradients of

morphogens identified during embryonic brain development and with genetic topography and spatiomolecular gradients. Our findings demonstrate the crucial role that comprehending the connectivity topographies and their genetic constraint plays in understanding the underlying principles that shape the human brain organization.

Global connectopies characterize the arealization consistent with genetic gradients

Our findings showed that the three global connectopies derived from the white matter partly characterized the embedding of connectivity architecture underlying the cortex in a low dimensional space organized along the dorsoventral, rostrocaudal, and mediolateral axes, which closely resemble the principal axes of brain development (*20, 58*) and the chemotactic gradients of early embryogenesis (*59, 60*). From a developmental perspective, both the encoding of chemical gradients by morphogens and the spatial expression patterns of all genes during the formation of the mature brain, along with recent research on phenotypic mapping facilitated by twin studies (*1-3*), indicate that gradient-based organizational principles may serve as one of the fundamental rules in the precise formation of gene-encoded connections and the establishment of functional cortical regions. Meanwhile, genes provide the initial blueprint that guides differentiation and the directional migration of neurons through the subsequent formation of different types of gradients of transcription factors, morphogens, etc., and, in parallel, the precise trajectory and projection of axons (*61*). However, the reality is likely somewhere in between that a few dozen molecules (rather than a few or a thousand) enact pattern formation rules to increase the probability that neurons make the correct connections. The global connectome organization might partly be governed by simple genetic rules. The scaffolding rule guides the exact formation of neural circuits (*62*), wherein genes might not drive the precise details of complex circuit diagrams but have the potential to influence their organizational rules during development (*23*). Here, the observed global connectopies could be one of the possible rules, consistent with the argument that anatomical connections could characterize the arealization and show consistency with cortical patterns driven by genetic profiles (*10, 63*).

The dorsoventral and rostrocaudal genetic topographies (Figure 4) observed in our study suggest genetic influences on cortical morphology where regional differentiation is controlled by genes expressing a graded pattern (*1, 2, 64, 65*). More interestingly, we not only observed a high correspondence between gene topology and our global connectopies, but also found that modules identified using global connectopies closely resemble that obtained using genetic correlation (*2*). This correspondence indicates the presence of the same graded pattern across the cortex at the genetic and connectional levels, and they are consistent with the gradation of architectonic features. The connectivity between cortical layers is related to their architectonic features and may provide evidence for the role of connections in the initial scaffolding for cortical organization. Previous research found that cortical patterning creates segregated areas with different functions via cell differentiation and migration. These segregated areas specifically occur along molecular gradients representing the patterned expression of morphogens and transcription factors (*18, 66*). We found that the genes related to the identified global connectopies coded for known morphogens and transcription factors (Figure 5). These factors were especially involved in biological processes, including regulation of transcription, metabolic process, morphogenesis, cellular development, and neuron projection. In addition, the genes associated with all the global connectopies were found to be more related to brain diseases. This finding is consistent with the observation that disruptions in forming early developmental gradients through mutations to gradient-associated genes can cause severe developmental disorders (*20, 67*). These associations demonstrated that global connectopies and their underlying genetic basis were essential to the development and function of the brain.

The morphogen gradients of the developing brain were previously established and found to radiate along the rostrocaudal, dorsoventral, and mediolateral axes of the neural compartment (*68*). These are conserved to maturity (*20*) and are consistent with our global connectopies (Figure

6A). At maturity, the morphogen gradients are replaced by a more distinct and discrete regional gene expression (*57*). Under the effect of morphogens secreted in the patterning centers with absolute positional information, numerous transcription factors are expressed in a graded manner. For example, the anterior expression of *FGF8* suppresses the posteriorly expressed transcription factors, resulting in their lower anterior but higher posterior expression (*69*). *FGF8* was also reported to stimulate the proliferation of cortical progenitor cells, thus regulating neurogenesis and arealization by thalamic axons (*70*). Similarly, manipulation of the transcription factor *EMX2* by genetic knockout resulted in finding higher expression posteromedially, as well as finding that a lower expression anterolaterally causes an expansion of the frontal and lateral regions at the expense of the visual cortex in mice (*71*). These transcription factors are believed to determine the areal fate and the expression of cell-surface molecules, thus determining the topographic organization of synaptic inputs and outputs (*1, 21*) and directing axonal outgrowth (*22*).

Many existing studies of thalamocortical and corticothalamic projections have identified specific receptors and ligands, such as the Eph receptor tyrosine kinases and their ephrin ligands, that are required to establish proper patterns of afferent and efferent cortical connectivity with subcortical structures (*72, 73*). However, whether these molecules play a similar role in instructing intracortical connectivity within the developing cortex is unclear. Relevant studies in this regard, such as *in utero* electroporation studies (*74*) and a study during primate development (*75*), suggest that directed axonal growth and target selection play a role in forming association projections between specific cortical areas. Moreover, according to the radial unit hypothesis of cortical development, radial glial cells in the embryonic brain facilitate the generation, placement, and allocation of neurons in the cortex and regulate how they wire up (*76, 77*). The radial glial scaffold might act as a “highway” for axons, facilitating their growth and ensuring their proper trajectories. Nevertheless, the factors that drive the competence of specific axons to grow into selected gray matter regions are unknown, but molecular interactions between axons and recipient cortical areas may be involved (*61*). Here, our current findings only identified associations between gene gradients and global connectopies in adult brains. Although we also did an integrated lifespan analysis of genes that appear to contribute to the connectopies, providing possible correlations, further studies are needed to explain the dynamics and causality during early development directly. In future studies, the progress of new technologies (*78, 79*) should be particularly helpful here and hopefully enable a clearer explanation of these relationships.

The global connectopies orchestrate flexible functions across the cortex

As the anatomical backbone of macroscale functional hierarchy, invariant white matter can scaffold many flexible cognitive processes. We demonstrated in this study that the dorsoventral, rostrocaudal, and mediolateral axes could provide new insights into the emergence of functions within this connected architecture.

The first, the dorsoventral global connectopy (GC1-DV), explained the greatest amount of variance. It had a similar topography to the second functional gradient (*28*), with the visual and sensorimotor cortex anchored at the two ends of the global connectopy. This was confirmed by the result of NeuroSynth decoding, i.e., the ventral and dorsal parts of the cortex were proposed to have different cognitive functions, with the dorsal part related to “foot” or “finger” and the ventral part linked to “navigation” or “episodic”, which corresponds to the distribution of the global connectopy on the intrinsic functional network. First, following the dual origin theory that the cerebral cortex evolved from two primordial brain structures and finally formed functionally distinct ventral and dorsal systems (*80, 81*), we identified the first principal component of the structural connection along the same axis. Pandya and others demonstrated that cortico-cortical connections are ordered consistently with the dorsoventral division and that long cortico-cortical tracts provide reciprocal pathways (*82-85*). More interestingly, the GC1-DV was related to the principal functional gradient found in neonates (*86*) and children (under 12 years old), which shifts to a pattern that transitions from the unimodal to the association cortex during development

(*87*). Since synaptogenesis and pruning in the unimodal cortex occur earlier, the association cortex goes through a protracted period of synaptic development with the formation of experience, memory, and semantics at a mature age (*88*, *89*) when the unimodal-association gradient emerges and becomes the principal functional gradient. This indicates that a stable structural connection might be the foundation of the functional organization of the cortex. Moreover, GC1-DV, varying along the sensory–association–motor axis, might be the place where the basic input-central processing-output information processing occurs. This change could be explained by changes in the dimensionality of multitask representations across this hierarchy, which are first compressed from the sensory to the association areas and then expanded from the association to the motor areas (Figure S18) (*90*). When we explored the white matter tracts that may contribute to the GC1-DV, we found that projection tracts, such as the thalamo-precentral tract and striato-occipital tract, contribute the most to the formation of the dorsoventral pattern. Because they are the sources of all external sensory information, the thalamocortical projections appeared in the earliest organisms, followed by the corpus callosum and association tracts in the mammalian brain (*91-94*).

For the second rostrocaudal global connectopy (GC2-RC), previous studies have provided converging evidence for the existence of the anterior-posterior axis. For example, neuron density decreases, and neuronal connectivity increases from the posterior to the anterior brain areas. This can be attributed to differences in neurogenesis between the posterior and anterior areas (*27*). These graded cytoarchitectural patterns reflect the local structural connection. When we studied the oscillational features of the brain, GC2-RC showed a remarkable relationship with several bands of MEG maps and had the same pattern as the spatial gradient of the dominant peak frequency of the oscillations (*95*). Since the cerebral cortex shows characteristic spectral activity patterns, with alpha activity strongest in occipitoparietal areas, beta activity strongest in sensorimotor areas, and delta and theta activity strongest in prefrontal brain areas (*96-98*), we suggest that global connectopies, as the anatomical structure, might shape the rhythmic neuronal activity of the brain, thus playing a central role in coordinating neuronal activity.

The third global connectopy, i.e., GC3-ML, which varied from the medial to the lateral areas, showed the most variation and, of the three global connectopies, had the highest correlation with inter-subject variance in functional connectivity (*99*). Considering the distance map from archicortical and paleocortical formations, the vertices on the cerebral cortex showed a distance from the two primordial brain structures along a medial-lateral axis, corresponding to the mediolateral axis during development. As to the tracts with high contributions of GC3-ML, except for the corpus callosum, the thalamo- and striato-cortical projections also project from the subcortical nuclei and reach different lateral cortices. Recent studies demonstrated that thalamic axons are routed to different cortical areas before entering the cortex by the organized interareal topography of thalamocortical projections in the ventral forebrain (*92*, *100*, *101*). These give evidence that topographically organized structural connections shape the process of development of the cerebral cortex into distinct cortical areas underlying different cognitive functions. Although various modalities of data obtained from different studies may introduce uncertainties and blurring of spatially organized features, we believe that high-quality data usage and group-level analysis will not affect the reliability of our findings.

Methodological consideration and future work

Several technical and methodological limitations must be acknowledged in the current work. The first and most direct concern is the accuracy of mapping structural connections using diffusion tensor imaging. However, diffusion tractography has been used as an irreplaceable tool to identify white matter across the brain *in vivo* and non-invasively, with certain limitations imposed by the tractography, such as gyral bias, which can cause false positive results (*102*, *103*). In the future, joint MRI and microscopy data analysis may help solve limitations (*104-106*). Alternatively, cutting-edge invasive neuro-techniques used in other mammalian cortexes, such as Cre-drivers for

cortical projection mapping (*107*) or polarised light imaging (*108, 109*), could be used at the mesoscale level of resolution to study whether such organizational axes are conserved across scales and species. The thresholding of the tractogram covariance and ignorance of negative edges should also be considered in the context of diffusion map embedding, which may convey potential interacting anatomical connectivity profiles but lack accommodation in the current method. Distance effect also needs to be considered when mapping the structural connectivity pattern, but the consistent genetic topography of the three global connectopies suggests that they are not distance-dependent. Interestingly, a recent study challenged traditional views and showed that the geometry of the brain had a more fundamental role in shaping its function than interregional connectivity (*110*). Although the association between cortical geometry and brain function should be recognized, the interacting role of connectopies and geometry deserves further attention to reveal the function realization of the developing human brain, especially the neonate brain. The underlying genetic drivers, which are the most essential and determining, should also be considered to explore the causal relationship between them. Secondly, the parcellation guided by the three global connectopies is very coarse compared with several fine-grained brain atlases that have been delineated using the gradient approach (*111, 112*). We did not utilize these more fine-grained parcels because we believe they are more likely to be shaped by local gradients compared with the three global connectopies, which characterize the global pattern across the brain.

In this study, we mainly focused on the structural connectivity patterns shown on the cortex and brought functional emergence into the discussion. More thorough microscale biological foundations and physiological processes were not explored here, but in future studies, they may aid in interpreting our findings about macroscale structural patterns. Since the spatiomolecular gradients expressed in childhood and adulthood have been established and shown to be consistent (*20*), an immediate goal will be to explore the transition in structural patterns throughout development. Whether these global connectopies are conserved across species could be another perspective to study when looking into the organization of the brain. We also need animal studies to validate or study the causal relationships between the genes, connectivity, and parcellations, which will reduce the impact of mismatch of ages and other factors resulting from relating HCP young adult diffusion MRI connectopies to AHBA-based gene expression information. Although the AHBA is the densest sample transcriptomic dataset of the human brain to date, it comes with the above-mentioned limitations, as well as the gap between post mortem changes in gene expression level and *in vivo* features, making our results a matter of caution. With the development of RNA sequencing technology, which enable rapid profiling and deep investigation of the transcriptome, more genes could be detected and provide valuable information (*113*). In addition, the observed organizing principles in the current work may also be used to guide the engineering of three-dimensional cortical spheroids and to comprehend the human-specific aspects of the neural circuit assembly (*114, 115*).

Conclusion

To conclude, we explored how genes link the accurate formation of connections despite significant differences in their numbers. Our research uncovered three determinant spatial trends across the cerebral cortex, aligning with the dorsoventral, rostrocaudal, and mediolateral axes, which we identified as global connectopies. These global connectopies were found to be aligned with the gradients of morphogens identified during embryonic brain development and with genetic topography and spatiomolecular gradients. Our findings revealed the existence of a low-dimensional, topological representation of brain connectivity that may share a common space with gene expression, providing a consistent characterization of the cortical arealization. We hope our discoveries will offer valuable insights into studying brain structure and function.

Materials and Methods

Data and preprocessing

Data collection We used a publicly available dataset containing 100 unrelated subjects (HCP-U100) (46 males; mean age, 29.11±3.67; age range, 22-36) provided by the Human Connectome Project (HCP) database (*33*) (http://www.humanconnectome.org/). All the scans and data from the individuals included in the study had passed the HCP quality control and assurance standards.

The scanning procedures and acquisition parameters were detailed in previous publications (*116*). In brief, T1w images were acquired with a 3D MPRAGE sequence on a Siemens 3T Skyra scanner equipped with a 32-channel head coil with the following parameters: TR = 2400 ms, TE = 2.14 ms, flip angle = 8°, FOV = 224×320 mm^2, voxel size = 0.7 mm isotropic. Diffusion data were acquired using single-shot 2D spin-echo multiband echo planar imaging on a Siemens 3 Tesla Skyra system (TR = 5520 ms, TE = 89.5 ms, flip angle = 78°, FOV = 210×180 mm). These consisted of three shells (b-values = 1000, 2000, and 3000 s/mm^2), with 90 diffusion directions isotropically distributed among each shell and six b = 0 acquisitions within each shell, with a spatial resolution of 1.25 mm isotropic voxels.

Image preprocessing The human T1w structural data had been preprocessed following the HCP's minimal preprocessing pipeline (*116*). In brief, the processing pipeline included imaging alignment to standard volume space using FSL, automatic anatomical surface reconstruction using FreeSurfer, and registration to a group average surface template space using the multi-modal surface matching (MSM) algorithm (*117*). Human volume data were registered to Montreal Neurological Institute (MNI) standard space, and surface data were transformed into surface template space (fs_LR).

The diffusion Images were processed using FDT (FMRIB's Diffusion Toolbox) of FSL. The main steps are normalization of the b0 image intensity across runs and correction for echo-planar imaging (EPI) susceptibility, eddy-current-induced distortions, gradient-nonlinearities, and subject motion. DTIFIT was then used to fit a diffusion tensor model. The probability distributions of the fiber orientation distribution were estimated using Bedpostx.

Next, skull-stripped T1-weighted images for each subject were co-registered to the subject's b0 images using FSL's FLIRT algorithm. Then nonlinear transformations between the T1 image and the MNI structural template were obtained using FSL's FNIRT. Based on concatenating these, we derived bi-directional transformations between the diffusion and MNI spaces.

Connectopy mapping

Tractography and connectivity blueprints To map the whole-brain connectivity pattern, we performed probabilistic tractography using FSL's probtrackx2 accelerated by using GPUs (*118, 119*). Specifically, the white surface was set as a seed region tracking to the rest of the brain with the ventricles removed and down-sampled to 3 mm resolution. The pial surface was used as a stop mask to prevent streamlines from crossing sulci. Each vertex was sampled 5000 times (5000 trackings) based on the orientation probability model for each voxel, with a curvature threshold of 0.2, a step length of 0.5 mm, and a number of steps of 3200. This resulted in a (*whole-surface vertices*) × (*whole-brain voxels*) matrix for further analysis. We checked the preprocessing images and tractography results of each subject to ensure the accuracy of our analysis. Specifically, the reconstructed surfaces were visually inspected, and transforms between different spaces were checked carefully. Tractography results were also visually checked to see if any streamline crosses the sulci.

We additionally created connectivity blueprints following previous work (*42*), which had been used to characterize connectivity patterns of brain regions or cortical vertices. Specifically, we first reconstructed 72 fiber bundles using a pre-trained deep-learning model, TractSeg (*41*), and down-sampled the resulting tract masks to 3 mm resolution, yielding a (*tracts*) × (*whole-brain voxels*) matrix. Then, the connectivity blueprints were generated by the product of this tract matrix, and the whole-brain connectivity matrix was obtained and normalized as described in the Tractography section. The columns of the resulting (*tracts*) × (*whole-surface vertices*) matrix

showed the connectivity distribution pattern of each cortical vertex, while the rows revealed the cortical termination patterns of the tracts.

Tractogram covariance analysis We calculated the tractogram covariance (TC) matrix to characterize the structural connectivity similarity profile. The vertex profiles underwent pairwise Pearson correlations, controlling for the average whole-cortex profile. For a given pair of vertices, *I* and *j*, TC was calculated as

$$TC(i,j) = \frac{r_{ij} - r_{ic}r_{jc}}{\sqrt{(1-r_{ic}^2)(1-r_{jc}^2)}}$$

in which r_{ij} was the Pearson correlation coefficient of the structural connectivity profile at vertices *I* and *j*, r_{ic} the correlation of the structural connectivity profile at vertex *I* with the average connectivity profile across the whole cortex, and r_{jc} the correlation of the structural connectivity profile at vertex *j* with the average connectivity profile across the entire cortex. A symmetric ~30k×30k TC matrix was produced for each subject. Then, the TC matrices of all subjects were averaged separately for the left and right hemispheres to get a group-level TC matrix for each hemisphere. In line with a previous study (*120*), the TC matrix was proportionally thresholded at 90% per row, with elements above zero retained to remove negative connections.

Connectopy decomposition The TC matrix was transformed into a non-negative square symmetric affinity matrix using a cosine affinity kernel. Then diffusion map embedding was implemented to identify the principal gradient components (*34*). Diffusion map embedding is a nonlinear manifold learning technique that maps cortical and cerebellar gradients (*28, 121*). Along these gradients, cortical vertices with similar connectivity profiles are embedded along the axis. Diffusion map embedding is relatively robust to noise and less computationally expensive than other nonlinear manifold learning techniques.

Global connectopies were computed separately for the left and right hemispheres with two key parameters: α controls the influence of the density of sampling points on the manifold, and t controls the scale of the eigenvalues. Here we set α=0.5 and t=0 as recommended (*28*). The amount of explained variance was assessed, and the first three global connectopies were chosen to map onto the cortical surface for further analysis. To discover whether low-dimensional connectivity blueprints could capture the structural connectivity information, we also generated global connectopies based on these connectivity blueprints using the same methods.

Individual global connectopies were calculated for each subject and aligned to the group GC with Procrustes rotation, which matches the order and direction of the global connectopies without scaling. The application of Procrustes rotation allows for comparison between individuals.

Relation to biological features To further validate the biological basis of the global connectopies, we mapped their distributions on atlases of laminar differentiation and cytoarchitectural classes. To this end, each vertex was assigned to one of four levels of laminar differentiation (i.e., idiotypic, unimodal, heteromodal, or paralimbic) (*35*) and one of the seven Von Economo/Koskinas cytoarchitectural classes (i.e., primary sensory, secondary sensory, motor, association 1, association 2, limbic, or insular) (*36*).

For the laminar differentiation maps, we referred to the map provided by a previous study (*122*). For the cytoarchitectural classes, Vertes et al. subdivided the DK atlas into 308 equal-sized ROIs of 500 mm^2 and assigned each region to one of the seven cytoarchitectural types according to the laminar structure of the cortex (*123*), with five types delineated by von Economo, that is, the primary motor cortex/precentral gyrus, two types association cortices, and secondary and primary sensory areas along with two additional subtypes: the limbic cortex (including the entorhinal, retrosplenial, presubicular and cingulate cortices, and thus primarily constitutes the allocortex) and the insular cortex. We then estimated the situation of each class along the global connectopy by the correspondence between the global connectopy value and the vertex class.

NeuroSynth term-based meta-analysis We projected the meta-analytical task-based activation along the global connectopies to investigate the association between functional decoding and our global connectopies. Here, we chose 590 terms related to specific cognitive processes that had been selected in previous publications (the full list of terms can be found in a previous publication (*124*)). The activation maps for the 590 cognitive terms were downloaded from the NeuroSynth database (https://neurosynth.org/). We generated 20 binarized masks at five-percentile increments of the global connectopy. Each of these 20 maps ranging from 0-5% to 95%-100%, were used as inputs to the subsequent meta-analysis. Each function term had a mean activation z-score per bin. Terms included in the visualization were those that had the highest two z-scores in each bin. A significance threshold of $z > 0.5$ was added as a visualization constraint.

Comparison to function-related brain maps To compare the brain maps, we estimated the correspondence of these brain maps to our global connectopies using Spearman rank correlation. Most of the brain maps were derived from the neuromaps distribution (*38*). Gradients of histology and microstructural profile covariance had also been computed previously (*120*), and the gradients of the neurotransmitters were from (*39*). Notably, the maps were obtained in their original coordinate system, so we converted them all to fsaverage_LR32k space. Spin tests (10000 times) were used to assess the correspondence between brain maps (*125*).

Note that the neurotransmitter data were only available for the "Schaefer-400" parcellation scheme before computing the correlation. Each parcel was assigned to the mean connectopy value across the vertices in the parcel, as in the other brain maps.

Projection of the global connectopies onto the white matter voxels We used general linear models (GLM) to project the global connectopies onto the white matter (*40*), exploring the contribution of each white matter voxel to the global connectopies. Specifically, we used the global connectopies as a dependent variable and the structural connection matrix as an independent variable. The resultant weights indicate the contribution of each white matter voxel. Note that the structural connection of each subject was obtained from probabilistic tractography in individual diffusion space. We registered each to MNI standard space and averaged, resulting in a group-level structural connection matrix.

Projection of the connectopies onto the white matter tracts To investigate how the global connectopies are related to the underlying white matter tracts, we made a tract projection map using the tract mask generated by TractSeg. Seventy-two tracts identified by TractSeg were grouped into five types for analysis: association tracts, commissural tracts, projection tracts, thalamo tracts, and striato tracts (Table S1). Using the connectivity blueprints we built before, we extracted the projection on the surface of each tract and calculated the mean value and variance using connectopy values of tract projection on the surface, thus revealing the relationship between the tracts and global connectopies. Due to the absence of projection on the surface, we excluded the superior cerebellar peduncle (SCP), middle cerebellar peduncle (MCP), and inferior cerebellar peduncle (ICP) from the study. We additionally removed Corpus Callosum – all because several segments were also reconstructed by TractSeg, i.e., CC_1 to CC_7.

Visualization of connectopies To inspect the global connectopies together intuitively, we plotted every two global connectopies in a 2D space and assigned them colors based on their positions. Then we generated RGB values for each vertex by normalizing three global connectopy values and mapped them on the surface, showing the dominant global connectopy at the vertex. Specifically, for the first gradient, values of all vertices were normalized from zero to one, resulting in a value of the red channel. The other two were conducted the same.

Hierarchical organization analysis

We implemented hierarchical clustering using global connectopies to test if the global connectopies could provide a descriptor of arealization. At the first level, the vertices were sorted in descending order from the first global connectopy. Brain regions were partitioned into two subregions based on the sign of the connectopy value. Furthermore, based on the positivity and

negativity of the second and third global connectopies, the whole cortex was partitioned into eight modules.

Gene analysis

Genetic correlation analysis of thickness and surface area We selected 194 twins from the HCP database (102 monozygotic and 92 dizygotic pairs; mean age, 29.96±2.96; age range, 22-36). The cortical surface was reconstructed to measure the cortical thickness and surface areas at each surface location using FreeSurfer in the fsaverage3 template to reduce computation time.

In a classical twin study of sets of MZ and DZ twins, four latent factors could account for the variance of any phenotype: additive genetic effects (A); non-additive genetic effects, including dominance (D); common or shared environmental effects (C); and non-shared or individual-specific environmental effects (*126*). Because of the minimal difference between the A and D effects, we fitted bivariate ACE models to compute the genetic correlations of the cortical thickness and surface area between two vertices of the cortex. Thus, the genetic covariance was calculated decomposed from the total phenotypic correlation. The analyses were performed using OpenMx (*127*).

Then we implemented diffusion map embedding on the genetic correlation matrix and compared it with the global connectopies. Genetic patterning results were obtained from previous studies (*1, 2*), which parcellated the cortex into four and twelve clusters. The parcellation results were compared with the modules derived from hierarchical clustering using the global connectopies.

AHBA data and preprocessing Regional microarray gene expression data were obtained from 6 postmortem brains (1 female, ages 24-57) provided by the Allen Human Brain Atlas (AHBA, https://human.brain-map.org/). The data were processed using the abagen toolbox (version 0.1.1; https://github.com/rmarkello/abagen) (*128*). First, the microarray probes were reannotated (*129*), and the probes that did not match a valid Entrez ID were excluded. Then, the probes were filtered based on their expression intensity relative to background noise, and the probes with the maximum summed adjacency for representing the corresponding gene expression were kept, yielding 15633 genes that corresponded to more than one probe. Last, we resampled the output gene expression map in fs5 space to fsaverage_LR32k space for subsequent study.

Gene enrichment analysis We used a prediction framework, partial least squares regression (PLSR), to determine the covariance between gene expression and global connectopies. Then we conducted 1000 bootstrapping to estimate the error of the weight of each gene. The normalized weight of each gene was denoted as the weight divided by the estimated error (*130*).

Genes were selected as the top and bottom 0.83% genes (n = 260) of each global connectopy's gene list, corrected for both tails and all three global connectopies for multiple comparisons. Each gene set combining both tails underwent gene ontology enrichment analyses. Gene sets that extended across the three global connectopies were also submitted to the analysis. ToppGene (https://toppgene.cchmc.org/), which contains the whole list of AHBA genes as the background gene set, was used to conduct the analysis. The following term categories were assessed: GO: Molecular Function, GO: Biological Process, GO: Cellular Component, Pathway, and Disease.

We collected gene expression data for all time points in the BrainSpan dataset to determine the developmental pattern of gene expression. Only genes associated with all three global connectopies were selected. Non-negative matrix factorization was used to derive the gene expression components for each macrostructure in the brain.

Global connectopy related gene analysis We further selected genes expressing the same pattern as any of the three global connectopies in AHBA (*57*). Each global connectopy was subdivided equally into ten parts, and two sample t-test was used to assess the difference of gene expression of selected genes between the first and the last bin (*131*).

Correspondence to spatiomolecular gradients Researchers recently reported three spatiomolecular gradients that retained the same pattern as morphogenetic gradients during their development. These gradients varied along three spatially embedded axes (*20*). We only used data from the left hemisphere because few samples in the AHBA were obtained from the right hemisphere. We replicated these molecular gradients at the ROI level with the "Schaefer-400" parcellation scheme and explored the correlation with the three global connectopies in this study.

Robustness analyses

Complementing our main analysis on calculating global connectopies, we examined the effect that may caused by age, sex, and brain size. For age, we divided subjects into three groups (age 20-25: n = 17; age 25-30: n = 40; age 30-35: n = 43). For sex, we divided the subjects into males (n=46) and females (n=54). For brain size, we extracted each HCP subject's total intracranial volume (TIV) from the Freesurfer output. Moreover, we divided into five groups (TIV 1.0-1.2: n = 3; TIV 1.2-1.4: n = 12; TIV 1.4-1.6: n = 38; TIV 1.6-1.8: n = 40; TIV 1.8-2.0: n = 7; [*106 mm3]). We calculated the correlation of the tractogram covariance matrix between groups.

We further derived the geodesic distance matrices on the mid-thickness surface of the human brain, calculated the gradients, and computed the correlation with global connectopies to test the effect by geodesic distance. We also remove short-range connections in the tractogram covariance matrices. We removed the value if the geodesic distance of the two vertices was less than 10mm, 20mm, and 30mm, respectively, and calculated the global connectopies again.

References

1. C. H. Chen, M. Fiecas, E. D. Gutierrez, M. S. Panizzon, L. T. Eyler, E. Vuoksimaa, W. K. Thompson, C. Fennema-Notestine, D. J. Hagler, Jr., T. L. Jernigan, M. C. Neale, C. E. Franz, M. J. Lyons, B. Fischl, M. T. Tsuang, A. M. Dale, W. S. Kremen, Genetic topography of brain morphology. *Proc Natl Acad Sci U S A* **110**, 17089-17094 (2013).
2. C. H. Chen, E. D. Gutierrez, W. Thompson, M. S. Panizzon, T. L. Jernigan, L. T. Eyler, C. Fennema-Notestine, A. J. Jak, M. C. Neale, C. E. Franz, M. J. Lyons, M. D. Grant, B. Fischl, L. J. Seidman, M. T. Tsuang, W. S. Kremen, A. M. Dale, Hierarchical genetic organization of human cortical surface area. *Science* **335**, 1634-1636 (2012).
3. C. H. Chen, M. S. Panizzon, L. T. Eyler, T. L. Jernigan, W. Thompson, C. Fennema-Notestine, A. J. Jak, M. C. Neale, C. E. Franz, S. Hamza, M. J. Lyons, M. D. Grant, B. Fischl, L. J. Seidman, M. T. Tsuang, W. S. Kremen, A. M. Dale, Genetic influences on cortical regionalization in the human brain. *Neuron* **72**, 537-544 (2011).
4. Y. Huang, Z. Wu, T. Li, X. Wang, Y. Wang, L. Xing, H. Zhu, W. Lin, L. Wang, L. Guo, J. H. Gilmore, G. Li, Mapping Genetic Topography of Cortical Thickness and Surface Area in Neonatal Brains. *J Neurosci*, (2023).
5. B. Zhao, T. Li, Z. Fan, Y. Yang, J. Shu, X. Yang, X. Wang, T. Luo, J. Tang, D. Xiong, Z. Wu, B. Li, J. Chen, Y. Shan, C. Tomlinson, Z. Zhu, Y. Li, J. L. Stein, H. Zhu, Heart-brain connections: Phenotypic and genetic insights from magnetic resonance images. *Science* **380**, abn6598 (2023).
6. J. B. Burt, M. Demirtas, W. J. Eckner, N. M. Navejar, J. L. Ji, W. J. Martin, A. Bernacchia, A. Anticevic, J. D. Murray, Hierarchy of transcriptomic specialization across human cortex captured by structural neuroimaging topography. *Nat Neurosci* **21**, 1251-1259 (2018).
7. L. C. Greig, M. B. Woodworth, M. J. Galazo, H. Padmanabhan, J. D. Macklis, Molecular logic of neocortical projection neuron specification, development and diversity. *Nat Rev Neurosci* **14**, 755-769 (2013).
8. Z. Molnar, G. J. Clowry, N. Sestan, A. Alzu'bi, T. Bakken, R. F. Hevner, P. S. Huppi, I. Kostovic, P. Rakic, E. S. Anton, D. Edwards, P. Garcez, A. Hoerder-Suabedissen, A.

Kriegstein, New insights into the development of the human cerebral cortex. *J Anat* **235**, 432-451 (2019).

9. K. Srinivasan, D. P. Leone, R. K. Bateson, G. Dobreva, Y. Kohwi, T. Kohwi-Shigematsu, R. Grosschedl, S. K. McConnell, A network of genetic repression and derepression specifies projection fates in the developing neocortex. *Proc Natl Acad Sci U S A* **109**, 19071-19078 (2012).
10. L. Fan, H. Li, J. Zhuo, Y. Zhang, J. Wang, L. Chen, Z. Yang, C. Chu, S. Xie, A. R. Laird, P. T. Fox, S. B. Eickhoff, C. Yu, T. Jiang, The Human Brainnetome Atlas: A New Brain Atlas Based on Connectional Architecture. *Cereb Cortex* **26**, 3508-3526 (2016).
11. R. E. Passingham, K. E. Stephan, R. Kotter, The anatomical basis of functional localization in the cortex. *Nat Rev Neurosci* **3**, 606-616 (2002).
12. U. Braun, A. Schafer, H. Walter, S. Erk, N. Romanczuk-Seiferth, L. Haddad, J. I. Schweiger, O. Grimm, A. Heinz, H. Tost, A. Meyer-Lindenberg, D. S. Bassett, Dynamic reconfiguration of frontal brain networks during executive cognition in humans. *Proc Natl Acad Sci U S A* **112**, 11678-11683 (2015).
13. Z. Cui, J. Stiso, G. L. Baum, J. Z. Kim, D. R. Roalf, R. F. Betzel, S. Gu, Z. Lu, C. H. Xia, X. He, R. Ciric, D. J. Oathes, T. M. Moore, R. T. Shinohara, K. Ruparel, C. Davatzikos, F. Pasqualetti, R. E. Gur, R. C. Gur, D. S. Bassett, T. D. Satterthwaite, Optimization of energy state transition trajectory supports the development of executive function during youth. *Elife* **9**, (2020).
14. S. Gu, F. Pasqualetti, M. Cieslak, Q. K. Telesford, A. B. Yu, A. E. Kahn, J. D. Medaglia, J. M. Vettel, M. B. Miller, S. T. Grafton, D. S. Bassett, Controllability of structural brain networks. *Nat Commun* **6**, 8414 (2015).
15. L. Talozzi, S. J. Forkel, V. Pacella, V. Nozais, E. Allart, C. Piscicelli, D. Perennou, D. Tranel, A. Boes, M. Corbetta, P. Nachev, M. Thiebaut de Schotten, Latent disconnectome prediction of long-term cognitive-behavioural symptoms in stroke. *Brain* **146**, 1963-1978 (2023).
16. M. Thiebaut de Schotten, C. Foulon, P. Nachev, Brain disconnections link structural connectivity with function and behaviour. *Nat Commun* **11**, 5094 (2020).
17. D. D. O'Leary, S. Sahara, Genetic regulation of arealization of the neocortex. *Curr Opin Neurobiol* **18**, 90-100 (2008).
18. C. R. Cadwell, A. Bhaduri, M. A. Mostajo-Radji, M. G. Keefe, T. J. Nowakowski, Development and Arealization of the Cerebral Cortex. *Neuron* **103**, 980-1004 (2019).
19. M. Hawrylycz, J. A. Miller, V. Menon, D. Feng, T. Dolbeare, A. L. Guillozet-Bongaarts, A. G. Jegga, B. J. Aronow, C. K. Lee, A. Bernard, M. F. Glasser, D. L. Dierker, J. Menche, A. Szafer, F. Collman, P. Grange, K. A. Berman, S. Mihalas, Z. Yao, L. Stewart, A. L. Barabasi, J. Schulkin, J. Phillips, L. Ng, C. Dang, D. R. Haynor, A. Jones, D. C. Van Essen, C. Koch, E. Lein, Canonical genetic signatures of the adult human brain. *Nat Neurosci* **18**, 1832-1844 (2015).
20. J. W. Vogel, A. Alexander-Bloch, K. Wagstyl, M. Bertolero, R. Markello, A. Pines, V. J. Sydnor, A. Diaz-Papkovich, J. Hansen, A. C. Evans, B. Bernhardt, B. Misic, T. Satterthwaite, J. Seidlitz, Conserved whole-brain spatiomolecular gradients shape adult brain functional organization. *bioRxiv*, (2022).
21. J. L. Rubenstein, P. Rakic, Genetic control of cortical development. *Cereb Cortex* **9**, 521-523 (1999).
22. J. K. Chilton, Molecular mechanisms of axon guidance. *Dev Biol* **292**, 13-24 (2006).
23. B. A. Hassan, P. R. Hiesinger, Beyond Molecular Codes: Simple Rules to Wire Complex Brains. *Cell* **163**, 285-291 (2015).
24. E. H. Shen, C. C. Overly, A. R. Jones, The Allen Human Brain Atlas: comprehensive gene expression mapping of the human brain. *Trends Neurosci* **35**, 711-714 (2012).

25. L. S. Mansour, Y. Tian, B. T. T. Yeo, V. Cropley, A. Zalesky, High-resolution connectomic fingerprints: Mapping neural identity and behavior. *Neuroimage* **229**, 117695 (2021).
26. P. N. Taylor, Y. Wang, M. Kaiser, Within brain area tractography suggests local modularity using high resolution connectomics. *Sci Rep* **7**, 39859 (2017).
27. J. M. Huntenburg, P. L. Bazin, D. S. Margulies, Large-Scale Gradients in Human Cortical Organization. *Trends Cogn Sci* **22**, 21-31 (2018).
28. D. S. Margulies, S. S. Ghosh, A. Goulas, M. Falkiewicz, J. M. Huntenburg, G. Langs, G. Bezgin, S. B. Eickhoff, F. X. Castellanos, M. Petrides, E. Jefferies, J. Smallwood, Situating the default-mode network along a principal gradient of macroscale cortical organization. *Proc Natl Acad Sci U S A* **113**, 12574-12579 (2016).
29. S. Atasoy, I. Donnelly, J. Pearson, Human brain networks function in connectome-specific harmonic waves. *Nat Commun* **7**, 10340 (2016).
30. M. G. Preti, D. Van De Ville, Decoupling of brain function from structure reveals regional behavioral specialization in humans. *Nat Commun* **10**, 4747 (2019).
31. P. A. Robinson, X. Zhao, K. M. Aquino, J. D. Griffiths, S. Sarkar, G. Mehta-Pandejee, Eigenmodes of brain activity: Neural field theory predictions and comparison with experiment. *Neuroimage* **142**, 79-98 (2016).
32. A. Tarun, D. Abramian, H. Behjat, D. Van De Ville, in *2019 IEEE 16th International Symposium on Biomedical Imaging (ISBI 2019)*. (IEEE, 2019), pp. 159-163.
33. D. C. Van Essen, S. M. Smith, D. M. Barch, T. E. Behrens, E. Yacoub, K. Ugurbil, W. U.-M. H. Consortium, The WU-Minn Human Connectome Project: an overview. *Neuroimage* **80**, 62-79 (2013).
34. R. R. Coifman, S. J. A. Lafon, c. h. analysis, Diffusion maps. **21**, 5-30 (2006).
35. M.-M. Mesulam, *Principles of behavioral and cognitive neurology* (Oxford University Press, 2000).
36. C. F. von Economo, G. N. Koskinas, L. C. Triarhou, *Atlas of cytoarchitectonics of the adult human cerebral cortex* (Karger Basel, 2008), vol. 10.
37. B. T. Yeo, F. M. Krienen, J. Sepulcre, M. R. Sabuncu, D. Lashkari, M. Hollinshead, J. L. Roffman, J. W. Smoller, L. Zollei, J. R. Polimeni, B. Fischl, H. Liu, R. L. Buckner, The organization of the human cerebral cortex estimated by intrinsic functional connectivity. *J Neurophysiol* **106**, 1125-1165 (2011).
38. R. D. Markello, J. Y. Hansen, Z. Q. Liu, V. Bazinet, G. Shafiei, L. E. Suarez, N. Blostein, J. Seidlitz, S. Baillet, T. D. Satterthwaite, M. M. Chakravarty, A. Raznahan, B. Misic, neuromaps: structural and functional interpretation of brain maps. *Nat Methods* **19**, 1472-1479 (2022).
39. J. Y. Hansen, G. Shafiei, R. D. Markello, K. Smart, S. M. L. Cox, M. Norgaard, V. Beliveau, Y. Wu, J. D. Gallezot, E. Aumont, S. Servaes, S. G. Scala, J. M. DuBois, G. Wainstein, G. Bezgin, T. Funck, T. W. Schmitz, R. N. Spreng, M. Galovic, M. J. Koepp, J. S. Duncan, J. P. Coles, T. D. Fryer, F. I. Aigbirhio, C. J. McGinnity, A. Hammers, J. P. Soucy, S. Baillet, S. Guimond, J. Hietala, M. A. Bedard, M. Leyton, E. Kobayashi, P. Rosa-Neto, M. Ganz, G. M. Knudsen, N. Palomero-Gallagher, J. M. Shine, R. E. Carson, L. Tuominen, A. Dagher, B. Misic, Mapping neurotransmitter systems to the structural and functional organization of the human neocortex. *Nat Neurosci* **25**, 1569-1581 (2022).
40. A. Tarun, H. Behjat, T. Bolton, D. Abramian, D. Van De Ville, Structural mediation of human brain activity revealed by white-matter interpolation of fMRI. *Neuroimage* **213**, 116718 (2020).
41. J. Wasserthal, P. Neher, K. H. Maier-Hein, TractSeg - Fast and accurate white matter tract segmentation. *Neuroimage* **183**, 239-253 (2018).

42. R. B. Mars, S. N. Sotiropoulos, R. E. Passingham, J. Sallet, L. Verhagen, A. A. Khrapitchev, N. Sibson, S. Jbabdi, Whole brain comparative anatomy using connectivity blueprints. *Elife* **7**, (2018).
43. D. J. Philp, M. S. Korgaonkar, S. M. Grieve, Thalamic volume and thalamo-cortical white matter tracts correlate with motor and verbal memory performance. *Neuroimage* **91**, 77-83 (2014).
44. P. L. Strick, The organization of thalamic inputs to the "premotor" areas. *Prog Brain Res* **64**, 99-109 (1986).
45. F. Janelle, C. Iorio-Morin, S. D'Amour, D. Fortin, Superior Longitudinal Fasciculus: A Review of the Anatomical Descriptions With Functional Correlates. *Front Neurol* **13**, 794618 (2022).
46. D. Koshiyama, M. Fukunaga, N. Okada, K. Morita, K. Nemoto, F. Yamashita, H. Yamamori, Y. Yasuda, J. Matsumoto, M. Fujimoto, N. Kudo, H. Azechi, Y. Watanabe, K. Kasai, R. Hashimoto, Association between the superior longitudinal fasciculus and perceptual organization and working memory: A diffusion tensor imaging study. *Neurosci Lett* **738**, 135349 (2020).
47. C. N. Adra, A. R. Iyengar, F. A. Syed, I. N. Kanaan, H. L. Rilo, W. Yu, R. Kheraj, S. R. Lin, T. Horiuchi, S. Khan, S. Weremowicz, B. Lim, C. C. Morton, D. R. Higgs, Human ARHGDIG, a GDP-dissociation inhibitor for Rho proteins: genomic structure, sequence, expression analysis, and mapping to chromosome 16p13.3. *Genomics* **53**, 104-109 (1998).
48. J. Arikkath, Molecular mechanisms of dendrite morphogenesis. *Front Cell Neurosci* **6**, 61 (2012).
49. C. A. Heyen, V. S. Tagliabracci, L. Zhai, P. J. Roach, Characterization of mouse UDP-glucose pyrophosphatase, a Nudix hydrolase encoded by the Nudt14 gene. *Biochem Biophys Res Commun* **390**, 1414-1418 (2009).
50. K. Krenke, K. Szczaluba, T. Bielecka, M. Rydzanicz, J. Lange, A. Koppolu, R. Ploski, FARSA mutations mimic phenylalanyl-tRNA synthetase deficiency caused by FARSB defects. *Clin Genet* **96**, 468-472 (2019).
51. L. Sansregret, A. Nepveu, The multiple roles of CUX1: insights from mouse models and cell-based assays. *Gene* **412**, 84-94 (2008).
52. F. Yang, R. De La Fuente, N. A. Leu, C. Baumann, K. J. McLaughlin, P. J. Wang, Mouse SYCP2 is required for synaptonemal complex assembly and chromosomal synapsis during male meiosis. *J Cell Biol* **173**, 497-507 (2006).
53. P. Zhu, W. Zhou, J. Wang, J. Puc, K. A. Ohgi, H. Erdjument-Bromage, P. Tempst, C. K. Glass, M. G. Rosenfeld, A histone H2A deubiquitinase complex coordinating histone acetylation and H1 dissociation in transcriptional regulation. *Mol Cell* **27**, 609-621 (2007).
54. K. Hendee, L. W. Wang, L. M. Reis, G. M. Rice, S. S. Apte, E. V. Semina, Identification and functional analysis of an ADAMTSL1 variant associated with a complex phenotype including congenital glaucoma, craniofacial, and other systemic features in a three-generation human pedigree. *Hum Mutat* **38**, 1485-1490 (2017).
55. S. Lu, R. Hernan, P. C. Marcogliese, Y. Huang, T. S. Gertler, M. Akcaboy, S. Liu, H. L. Chung, X. Pan, X. Sun, M. M. Oguz, U. Oztoprak, J. H. F. de Baaij, J. Ivanisevic, E. McGinnis, M. J. Guillen Sacoto, W. K. Chung, H. J. Bellen, Loss-of-function variants in TIAM1 are associated with developmental delay, intellectual disability, and seizures. *Am J Hum Genet* **109**, 571-586 (2022).
56. Q. Ru, Y. Lu, A. B. Saifullah, F. A. Blanco, C. Yao, J. P. Cata, D. P. Li, K. F. Tolias, L. Li, TIAM1-mediated synaptic plasticity underlies comorbid depression-like and ketamine antidepressant-like actions in chronic pain. *J Clin Invest* **132**, (2022).
57. P. Rakic, A. E. Ayoub, J. J. Breunig, M. H. Dominguez, Decision by division: making cortical maps. *Trends Neurosci* **32**, 291-301 (2009).

58. E. Takahashi, R. D. Folkerth, A. M. Galaburda, P. E. Grant, Emerging cerebral connectivity in the human fetal brain: an MR tractography study. *Cereb Cortex* **22**, 455-464 (2012).
59. P. J. Van Haastert, P. N. Devreotes, Chemotaxis: signalling the way forward. *Nat Rev Mol Cell Biol* **5**, 626-634 (2004).
60. D. Wu, Signaling mechanisms for regulation of chemotaxis. *Cell Res* **15**, 52-56 (2005).
61. R. J. Kast, P. Levitt, Precision in the development of neocortical architecture: From progenitors to cortical networks. *Prog Neurobiol* **175**, 77-95 (2019).
62. M. Langen, E. Agi, D. J. Altschuler, L. F. Wu, S. J. Altschuler, P. R. Hiesinger, The Developmental Rules of Neural Superposition in Drosophila. *Cell* **162**, 120-133 (2015).
63. Y. Cui, B. Liu, Y. Zhou, L. Fan, J. Li, Y. Zhang, H. Wu, B. Hou, C. Wang, F. Zheng, C. Qiu, L. L. Rao, Y. Ning, S. Li, T. Jiang, Genetic Effects on Fine-Grained Human Cortical Regionalization. *Cereb Cortex* **26**, 3732-3743 (2016).
64. S. L. Valk, T. Xu, D. S. Margulies, S. K. Masouleh, C. Paquola, A. Goulas, P. Kochunov, J. Smallwood, B. T. T. Yeo, B. C. Bernhardt, S. B. Eickhoff, Shaping brain structure: Genetic and phylogenetic axes of macroscale organization of cortical thickness. *Sci Adv* **6**, (2020).
65. S. Yang, K. Wagstyl, Y. Meng, X. Zhao, J. Li, P. Zhong, B. Li, Y. S. Fan, H. Chen, W. Liao, Cortical patterning of morphometric similarity gradient reveals diverged hierarchical organization in sensory-motor cortices. *Cell Rep* **36**, 109582 (2021).
66. S. N. Sansom, F. J. Livesey, Gradients in the brain: the control of the development of form and function in the cerebral cortex. *Cold Spring Harb Perspect Biol* **1**, a002519 (2009).
67. L. Flores-Sarnat, H. B. Sarnat, Axes and gradients of the neural tube for a morphological/molecular genetic classification of nervous system malformations. *Handb Clin Neurol* **87**, 1-11 (2008).
68. R. V. Hoch, J. L. Rubenstein, S. Pleasure, Genes and signaling events that establish regional patterning of the mammalian forebrain. *Semin Cell Dev Biol* **20**, 378-386 (2009).
69. E. E. Storm, S. Garel, U. Borello, J. M. Hebert, S. Martinez, S. K. McConnell, G. R. Martin, J. L. Rubenstein, Dose-dependent functions of Fgf8 in regulating telencephalic patterning centers. *Development* **133**, 1831-1844 (2006).
70. T. Sun, R. F. Hevner, Growth and folding of the mammalian cerebral cortex: from molecules to malformations. *Nat Rev Neurosci* **15**, 217-232 (2014).
71. T. Hamasaki, A. Leingartner, T. Ringstedt, D. D. O'Leary, EMX2 regulates sizes and positioning of the primary sensory and motor areas in neocortex by direct specification of cortical progenitors. *Neuron* **43**, 359-372 (2004).
72. J. Bolz, D. Uziel, S. Muhlfriedel, A. Gullmar, C. Peuckert, K. Zarbalis, W. Wurst, M. Torii, P. Levitt, Multiple roles of ephrins during the formation of thalamocortical projections: maps and more. *J Neurobiol* **59**, 82-94 (2004).
73. P. P. Gao, Y. Yue, J. H. Zhang, D. P. Cerretti, P. Levitt, R. Zhou, Regulation of thalamic neurite outgrowth by the Eph ligand ephrin-A5: implications in the development of thalamocortical projections. *Proc Natl Acad Sci U S A* **95**, 5329-5334 (1998).
74. L. R. Fenlon, R. Suarez, L. J. Richards, The anatomy, organisation and development of contralateral callosal projections of the mouse somatosensory cortex. *Brain Neurosci Adv* **1**, 2398212817694888 (2017).
75. P. Barone, C. Dehay, M. Berland, H. Kennedy, Role of directed growth and target selection in the formation of cortical pathways: prenatal development of the projection of area V2 to area V4 in the monkey. *J Comp Neurol* **374**, 1-20 (1996).
76. C. R. Casingal, K. D. Descant, E. S. Anton, Coordinating cerebral cortical construction and connectivity: Unifying influence of radial progenitors. *Neuron* **110**, 1100-1115 (2022).

77. T. J. Nowakowski, A. A. Pollen, C. Sandoval-Espinosa, A. R. Kriegstein, Transformation of the Radial Glia Scaffold Demarcates Two Stages of Human Cerebral Cortex Development. *Neuron* **91**, 1219-1227 (2016).
78. F. Marsoner, P. Koch, J. Ladewig, Cortical organoids: why all this hype? *Curr Opin Genet Dev* **52**, 22-28 (2018).
79. G. Quadrato, P. Arlotta, Present and future of modeling human brain development in 3D organoids. *Curr Opin Cell Biol* **49**, 47-52 (2017).
80. R. G. Giaccio, The dual origin hypothesis: an evolutionary brain-behavior framework for analyzing psychiatric disorders. *Neurosci Biobehav Rev* **30**, 526-550 (2006).
81. D. Pandya, B. Seltzer, M. Petrides, P. B. Cipolloni, *Cerebral Cortex: Architecture, Connections, and the Dual Origin Concept* (Oxford University Press, 2015).
82. D. N. Pandya, B. Seltzer, Intrinsic connections and architectonics of posterior parietal cortex in the rhesus monkey. *J Comp Neurol* **204**, 196-210 (1982).
83. D. N. Pandya, B. Seltzer, H. Barbas, Input-output organization of the primate cerebral cortex. (1986).
84. M. Petrides, D. N. Pandya, Dorsolateral prefrontal cortex: comparative cytoarchitectonic analysis in the human and the macaque brain and corticocortical connection patterns. *Eur J Neurosci* **11**, 1011-1036 (1999).
85. M. Petrides, D. N. Pandya, Comparative cytoarchitectonic analysis of the human and the macaque ventrolateral prefrontal cortex and corticocortical connection patterns in the monkey. *Eur J Neurosci* **16**, 291-310 (2002).
86. S. Lariviere, R. Vos de Wael, S. J. Hong, C. Paquola, S. Tavakol, A. J. Lowe, D. V. Schrader, B. C. Bernhardt, Multiscale Structure-Function Gradients in the Neonatal Connectome. *Cereb Cortex* **30**, 47-58 (2020).
87. H. M. Dong, D. S. Margulies, X. N. Zuo, A. J. Holmes, Shifting gradients of macroscale cortical organization mark the transition from childhood to adolescence. *Proc Natl Acad Sci U S A* **118**, (2021).
88. P. R. Huttenlocher, Synaptic density in human frontal cortex - developmental changes and effects of aging. *Brain Res* **163**, 195-205 (1979).
89. P. R. Huttenlocher, C. De Courten, L. J. Garey, H. Van der Loos, Synaptic development in human cerebral cortex. *Int J Neurol* **16-17**, 144-154 (1982).
90. T. Ito, J. D. Murray, Multitask representations in the human cortex transform along a sensory-to-motor hierarchy. *Nat Neurosci*, (2022).
91. C. Auladell, P. Perez-Sust, H. Super, E. Soriano, The early development of thalamocortical and corticothalamic projections in the mouse. *Anat Embryol (Berl)* **201**, 169-179 (2000).
92. J. C. Hohl-Abrahao, O. D. Creutzfeldt, Topographical mapping of the thalamocortical projections in rodents and comparison with that in primates. *Exp Brain Res* **87**, 283-294 (1991).
93. R. Olivares, J. Montiel, F. Aboitiz, Species differences and similarities in the fine structure of the mammalian corpus callosum. *Brain Behav Evol* **57**, 98-105 (2001).
94. S. Velut, C. Destrieux, M. Kakou, [Morphologic anatomy of the corpus callosum]. *Neurochirurgie* **44**, 17-30 (1998).
95. K. Mahjoory, J. M. Schoffelen, A. Keitel, J. Gross, The frequency gradient of human resting-state brain oscillations follows cortical hierarchies. *Elife* **9**, (2020).
96. A. Hillebrand, P. Tewarie, E. van Dellen, M. Yu, E. W. Carbo, L. Douw, A. A. Gouw, E. C. van Straaten, C. J. Stam, Direction of information flow in large-scale resting-state networks is frequency-dependent. *Proc Natl Acad Sci U S A* **113**, 3867-3872 (2016).
97. A. Keitel, J. Gross, Individual Human Brain Areas Can Be Identified from Their Characteristic Spectral Activation Fingerprints. *PLoS Biol* **14**, e1002498 (2016).

98. M. S. Mellem, S. Wohltjen, S. J. Gotts, A. S. Ghuman, A. Martin, Intrinsic frequency biases and profiles across human cortex. *J Neurophysiol* **118**, 2853-2864 (2017).
99. S. Mueller, D. Wang, M. D. Fox, B. T. Yeo, J. Sepulcre, M. R. Sabuncu, R. Shafee, J. Lu, H. Liu, Individual variability in functional connectivity architecture of the human brain. *Neuron* **77**, 586-595 (2013).
100. A. W. Powell, T. Sassa, Y. Wu, M. Tessier-Lavigne, F. Polleux, Topography of thalamic projections requires attractive and repulsive functions of Netrin-1 in the ventral telencephalon. *PLoS Biol* **6**, e116 (2008).
101. P. Vanderhaeghen, F. Polleux, Developmental mechanisms patterning thalamocortical projections: intrinsic, extrinsic and in between. *Trends Neurosci* **27**, 384-391 (2004).
102. K. H. Maier-Hein, P. F. Neher, J. C. Houde, M. A. Cote, E. Garyfallidis, J. Zhong, M. Chamberland, F. C. Yeh, Y. C. Lin, Q. Ji, W. E. Reddick, J. O. Glass, D. Q. Chen, Y. Feng, C. Gao, Y. Wu, J. Ma, R. He, Q. Li, C. F. Westin, S. Deslauriers-Gauthier, J. O. O. Gonzalez, M. Paquette, S. St-Jean, G. Girard, F. Rheault, J. Sidhu, C. M. W. Tax, F. Guo, H. Y. Mesri, S. David, M. Froeling, A. M. Heemskerk, A. Leemans, A. Bore, B. Pinsard, C. Bedetti, M. Desrosiers, S. Brambati, J. Doyon, A. Sarica, R. Vasta, A. Cerasa, A. Quattrone, J. Yeatman, A. R. Khan, W. Hodges, S. Alexander, D. Romascano, M. Barakovic, A. Auria, O. Esteban, A. Lemkaddem, J. P. Thiran, H. E. Cetingul, B. L. Odry, B. Mailhe, M. S. Nadar, F. Pizzagalli, G. Prasad, J. E. Villalon-Reina, J. Galvis, P. M. Thompson, F. S. Requejo, P. L. Laguna, L. M. Lacerda, R. Barrett, F. Dell'Acqua, M. Catani, L. Petit, E. Caruyer, A. Daducci, T. B. Dyrby, T. Holland-Letz, C. C. Hilgetag, B. Stieltjes, M. Descoteaux, The challenge of mapping the human connectome based on diffusion tractography. *Nat Commun* **8**, 1349 (2017).
103. C. Reveley, A. K. Seth, C. Pierpaoli, A. C. Silva, D. Yu, R. C. Saunders, D. A. Leopold, F. Q. Ye, Superficial white matter fiber systems impede detection of long-range cortical connections in diffusion MR tractography. *Proc Natl Acad Sci U S A* **112**, E2820-2828 (2015).
104. M. Axer, K. Amunts, Scale matters: The nested human connectome. *Science* **378**, 500-504 (2022).
105. A. F. Howard, I. N. Huszar, A. Smart, M. Cottaar, G. Daubney, T. Hanayik, A. A. Khrapitchev, R. B. Mars, J. Mollink, C. Scott, N. R. Sibson, J. Sallet, S. Jbabdi, K. L. Miller, The BigMac dataset: an open resource combining multi-contrast MRI and microscopy in the macaque brain. *bioRxiv*, (2022).
106. S. Y. Huang, T. Witzel, B. Keil, A. Scholz, M. Davids, P. Dietz, E. Rummert, R. Ramb, J. E. Kirsch, A. Yendiki, Q. Fan, Q. Tian, G. Ramos-Llorden, H. H. Lee, A. Nummenmaa, B. Bilgic, K. Setsompop, F. Wang, A. V. Avram, M. Komlosh, D. Benjamini, K. N. Magdoom, S. Pathak, W. Schneider, D. S. Novikov, E. Fieremans, S. Tounekti, C. Mekkaoui, J. Augustinack, D. Berger, A. Shapson-Coe, J. Lichtman, P. J. Basser, L. L. Wald, B. R. Rosen, Connectome 2.0: Developing the next-generation ultra-high gradient strength human MRI scanner for bridging studies of the micro-, meso- and macro-connectome. *Neuroimage* **243**, 118530 (2021).
107. J. A. Harris, S. Mihalas, K. E. Hirokawa, J. D. Whitesell, H. Choi, A. Bernard, P. Bohn, S. Caldejon, L. Casal, A. Cho, A. Feiner, D. Feng, N. Gaudreault, C. R. Gerfen, N. Graddis, P. A. Groblewski, A. M. Henry, A. Ho, R. Howard, J. E. Knox, L. Kuan, X. Kuang, J. Lecoq, P. Lesnar, Y. Li, J. Luviano, S. McConoughey, M. T. Mortrud, M. Naeemi, L. Ng, S. W. Oh, B. Ouellette, E. Shen, S. A. Sorensen, W. Wakeman, Q. Wang, Y. Wang, A. Williford, J. W. Phillips, A. R. Jones, C. Koch, H. Zeng, Hierarchical organization of cortical and thalamic connectivity. *Nature* **575**, 195-202 (2019).

108. M. Axer, K. Amunts, D. Grassel, C. Palm, J. Dammers, H. Axer, U. Pietrzyk, K. Zilles, A novel approach to the human connectome: ultra-high resolution mapping of fiber tracts in the brain. *Neuroimage* **54**, 1091-1101 (2011).
109. H. Wang, C. Magnain, R. Wang, J. Dubb, A. Varjabedian, L. S. Tirrell, A. Stevens, J. C. Augustinack, E. Konukoglu, I. Aganj, M. P. Frosch, J. D. Schmahmann, B. Fischl, D. A. Boas, as-PSOCT: Volumetric microscopic imaging of human brain architecture and connectivity. *Neuroimage* **165**, 56-68 (2018).
110. J. C. Pang, K. M. Aquino, M. Oldehinkel, P. A. Robinson, B. D. Fulcher, M. Breakspear, A. Fornito, Geometric constraints on human brain function. *Nature*, (2023).
111. E. M. Gordon, T. O. Laumann, B. Adeyemo, J. F. Huckins, W. M. Kelley, S. E. Petersen, Generation and Evaluation of a Cortical Area Parcellation from Resting-State Correlations. *Cereb Cortex* **26**, 288-303 (2016).
112. A. Schaefer, R. Kong, E. M. Gordon, T. O. Laumann, X. N. Zuo, A. J. Holmes, S. B. Eickhoff, B. T. T. Yeo, Local-Global Parcellation of the Human Cerebral Cortex from Intrinsic Functional Connectivity MRI. *Cereb Cortex* **28**, 3095-3114 (2018).
113. Z. Wang, M. Gerstein, M. Snyder, RNA-Seq: a revolutionary tool for transcriptomics. *Nat Rev Genet* **10**, 57-63 (2009).
114. Y. Miura, M. Y. Li, O. Revah, S. J. Yoon, G. Narazaki, S. P. Pasca, Engineering brain assembloids to interrogate human neural circuits. *Nat Protoc* **17**, 15-35 (2022).
115. S. A. Sloan, J. Andersen, A. M. Pasca, F. Birey, S. P. Pasca, Generation and assembly of human brain region-specific three-dimensional cultures. *Nat Protoc* **13**, 2062-2085 (2018).
116. M. F. Glasser, S. N. Sotiropoulos, J. A. Wilson, T. S. Coalson, B. Fischl, J. L. Andersson, J. Xu, S. Jbabdi, M. Webster, J. R. Polimeni, D. C. Van Essen, M. Jenkinson, W. U.-M. H. Consortium, The minimal preprocessing pipelines for the Human Connectome Project. *Neuroimage* **80**, 105-124 (2013).
117. E. C. Robinson, S. Jbabdi, M. F. Glasser, J. Andersson, G. C. Burgess, M. P. Harms, S. M. Smith, D. C. Van Essen, M. Jenkinson, MSM: a new flexible framework for Multimodal Surface Matching. *Neuroimage* **100**, 414-426 (2014).
118. T. E. Behrens, H. J. Berg, S. Jbabdi, M. F. Rushworth, M. W. Woolrich, Probabilistic diffusion tractography with multiple fibre orientations: What can we gain? *Neuroimage* **34**, 144-155 (2007).
119. M. Hernandez-Fernandez, I. Reguly, S. Jbabdi, M. Giles, S. Smith, S. N. Sotiropoulos, Using GPUs to accelerate computational diffusion MRI: From microstructure estimation to tractography and connectomes. *Neuroimage* **188**, 598-615 (2019).
120. C. Paquola, R. Vos De Wael, K. Wagstyl, R. A. I. Bethlehem, S. J. Hong, J. Seidlitz, E. T. Bullmore, A. C. Evans, B. Misic, D. S. Margulies, J. Smallwood, B. C. Bernhardt, Microstructural and functional gradients are increasingly dissociated in transmodal cortices. *PLoS Biol* **17**, e3000284 (2019).
121. X. Guell, J. D. Schmahmann, J. Gabrieli, S. S. Ghosh, Functional gradients of the cerebellum. *Elife* **7**, (2018).
122. C. Paquola, R. A. Bethlehem, J. Seidlitz, K. Wagstyl, R. Romero-Garcia, K. J. Whitaker, R. Vos de Wael, G. B. Williams, N. Consortium, P. E. Vertes, D. S. Margulies, B. Bernhardt, E. T. Bullmore, Shifts in myeloarchitecture characterise adolescent development of cortical gradients. *Elife* **8**, (2019).
123. P. E. Vertes, T. Rittman, K. J. Whitaker, R. Romero-Garcia, F. Vasa, M. G. Kitzbichler, K. Wagstyl, P. Fonagy, R. J. Dolan, P. B. Jones, I. M. Goodyer, N. Consortium, E. T. Bullmore, Gene transcription profiles associated with inter-modular hubs and connection distance in human functional magnetic resonance imaging networks. *Philos Trans R Soc Lond B Biol Sci* **371**, (2016).

124. V. R. Karolis, M. Corbetta, M. Thiebaut de Schotten, The architecture of functional lateralisation and its relationship to callosal connectivity in the human brain. *Nat Commun* **10**, 1417 (2019).
125. A. F. Alexander-Bloch, H. Shou, S. Liu, T. D. Satterthwaite, D. C. Glahn, R. T. Shinohara, S. N. Vandekar, A. Raznahan, On testing for spatial correspondence between maps of human brain structure and function. *Neuroimage* **178**, 540-551 (2018).
126. M. C. Neale, L. R. Cardon, Methodology for genetic studies of twins and families. *Springer Science & Business Media* **67**, (2013).
127. M. C. Neale, M. D. Hunter, J. N. Pritikin, M. Zahery, T. R. Brick, R. M. Kirkpatrick, R. Estabrook, T. C. Bates, H. H. Maes, S. M. Boker, OpenMx 2.0: Extended Structural Equation and Statistical Modeling. *Psychometrika* **81**, 535-549 (2016).
128. R. D. Markello, A. Arnatkeviciute, J. B. Poline, B. D. Fulcher, A. Fornito, B. Misic, Standardizing workflows in imaging transcriptomics with the abagen toolbox. *Elife* **10**, (2021).
129. A. Arnatkeviciute, B. D. Fulcher, A. Fornito, A practical guide to linking brain-wide gene expression and neuroimaging data. *Neuroimage* **189**, 353-367 (2019).
130. S. E. Morgan, J. Seidlitz, K. J. Whitaker, R. Romero-Garcia, N. E. Clifton, C. Scarpazza, T. van Amelsvoort, M. Marcelis, J. van Os, G. Donohoe, D. Mothersill, A. Corvin, A. Pocklington, A. Raznahan, P. McGuire, P. E. Vertes, E. T. Bullmore, Cortical patterning of abnormal morphometric similarity in psychosis is associated with brain expression of schizophrenia-related genes. *Proc Natl Acad Sci U S A* **116**, 9604-9609 (2019).
131. A. M. Fjell, C. H. Chen, D. Sederevicius, M. H. Sneve, H. Grydeland, S. K. Krogsrud, I. Amlien, L. Ferschmann, H. Ness, L. Folvik, D. Beck, A. M. Mowinckel, C. K. Tamnes, R. Westerhausen, A. K. Haberg, A. M. Dale, K. B. Walhovd, Continuity and Discontinuity in Human Cortical Development and Change From Embryonic Stages to Old Age. *Cereb Cortex* **29**, 3879-3890 (2019).

Acknowledgments
The authors appreciate the English language and editing assistance of Rhoda E. and Edmund F. Perozzi, PhDs. Data were provided by the Human Connectome Project, WU-Minn Consortium (Principal Investigators: David Van Essen and Kamil Ugurbil; 1U54MH091657) funded by the 16 NIH Institutes and Centers that support the NIH Blueprint for Neuroscience Research; and by the McDonnell Center for Systems Neuroscience at Washington University.

Funding: This work was partially supported by
STI2030-Major Projects: Grant No. 2021ZD0200200 (LF)
Natural Science Foundation of China: Grant No. 82072099 (LF)
Natural Science Foundation of China: Grant No. 62250058 (CC)

Competing interest: The authors declare no competing interest.

Data and materials availability:
Data from the Human Connectome Project can be downloaded at https://db.humanconnectome.org/. The activated maps of cognitive terms can be downloaded from the NeuroSynth database (https://neurosynth.org/). The human gene expression data are available in the Allen Brain Atlas (https://human.brain-map.org/static/download). Data from BrainSpan can be downloaded at https://www.brainspan.org/. The HCP pipeline can be found at https://github.com/WashingtonUniversity/HCPpipelines. The neuroimaging preprocessing software used for the other datasets is freely available (FreeSurfer v6.0,

http://surfer.nmr.mgh.harvard.edu/, and FSL v6.0.5, https://fsl.fmrib.ox.ac.uk/fsl/fslwiki). The gene processing pipeline is available (abagen, https://github.com/rmarkello/abagen), and gene enrichment analysis is conducted at https://toppgene.cchmc.org/. The brain maps were presented using BrainSpace (https://brainspace.readthedocs.io/) and Workbench v1.5.0 (https://www.humanconnectome.org/software/connectome-workbench). The tracts were visualized using BrainNet Viewer v1.7 (https://www.nitrc.org/projects/bnv/).

Figures and Tables

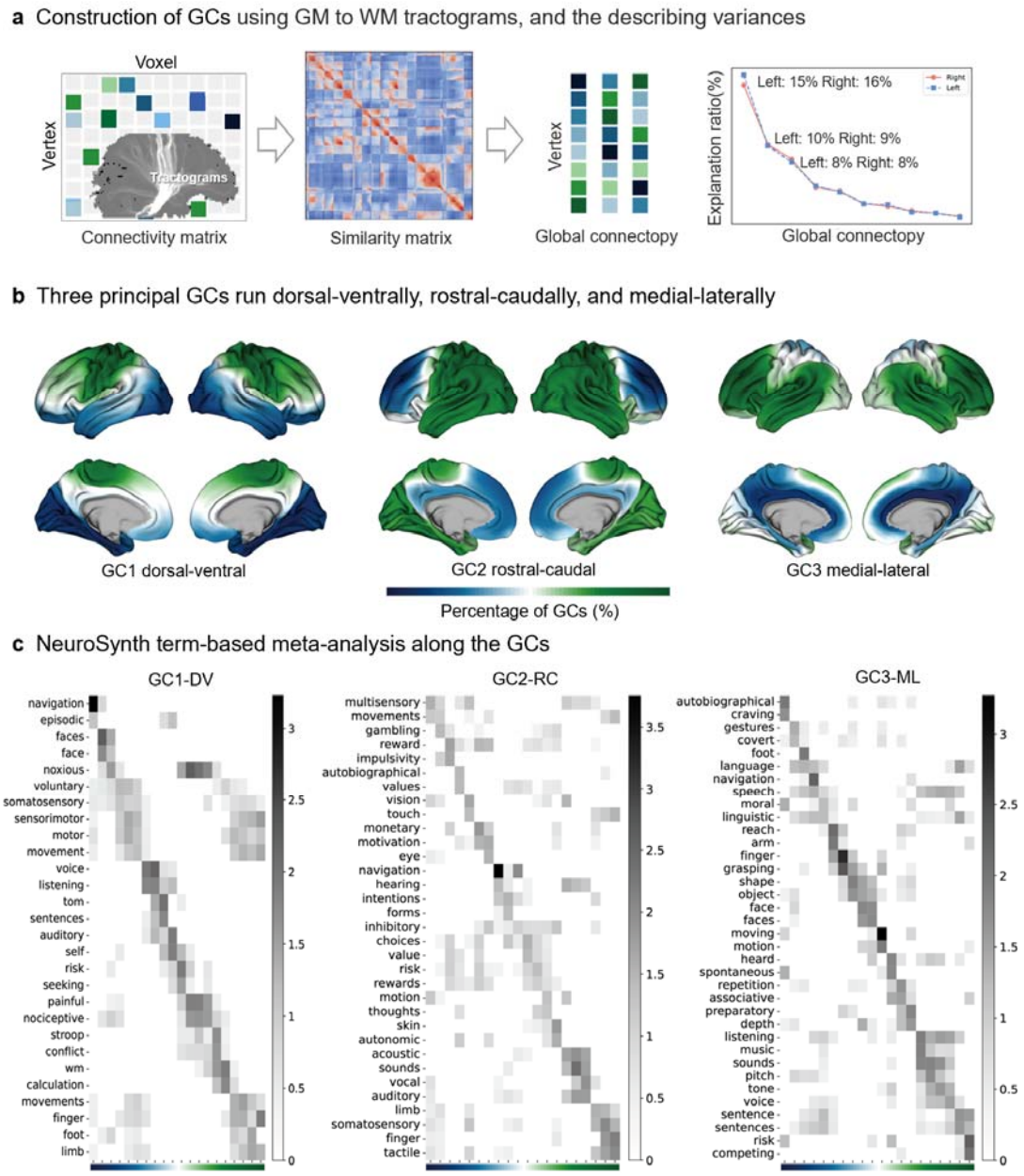

Figure 1. Three global connectopies in the human cerebral cortex. (a) The construction of global connectopies. White matter tractograms were calculated to get a similarity matrix, i.e., a tractogram covariance (TC) matrix. Diffusion embedding was implemented on the TC matrix, resulting in low-dimensional gradients. A scree plot describing variance is shown on the right. **(b)** The first three global connectopies ran dorsoventrally, rostrocaudally, and mediolaterally and were termed GC1-DV, GC2-RC, and GC3-ML, respectively. **(c)** NeuroSynth term-based meta-

analysis along the global connectopies. Terms that had the highest two z-scores for each binarized mask of the global connectopies were included in this visualization.

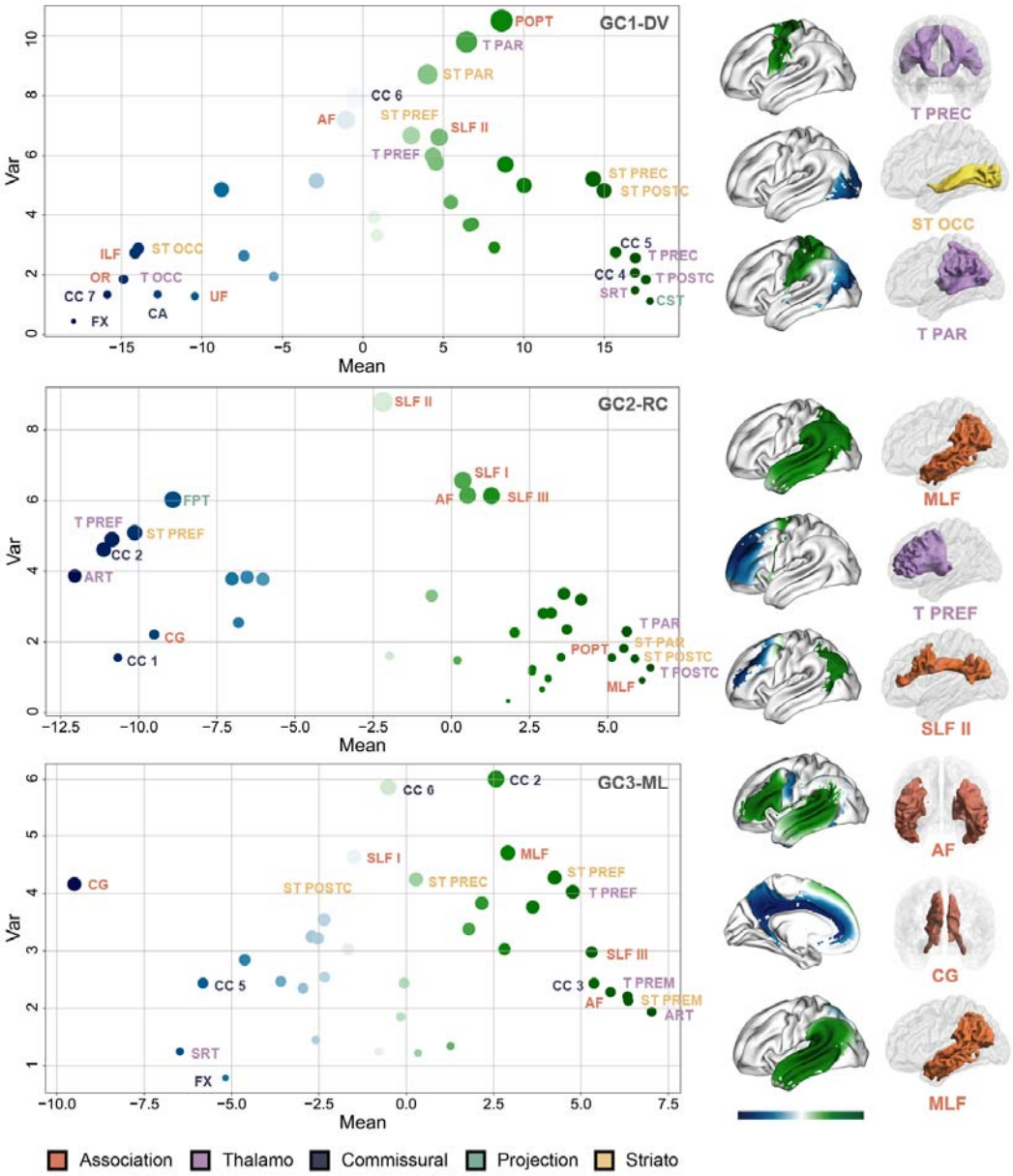

Figure 2. The three global connectopies are situated by distinct sets of white matter tracts. Mean values and variances of the contribution of five types of tracts to the global connectopies are shown. Each dot represents one tract. Different colors represented different types of tracts, with deeper colors for higher contributions. The right two columns show two types of characteristic tracts contributing to the global connectopies, with one type of tract situated at one extreme of the global connectopy and the other stretched across the global connectopy. The first column shows the cortical projection on the surface of the tract, and the second shows the corresponding fiber bundles reconstructed by TractSeg.

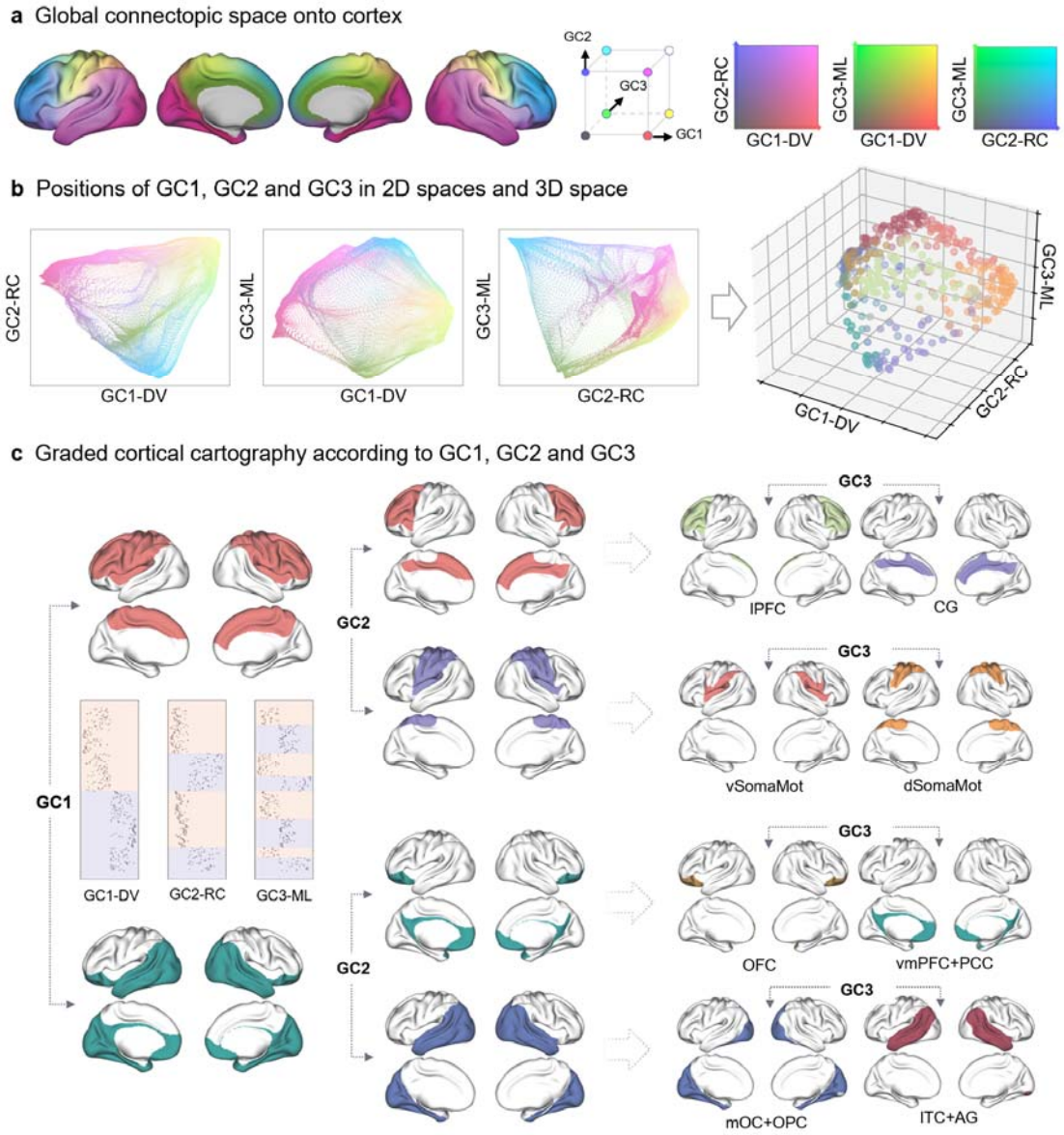

Figure 3. Global connectopies provide a large-scale descriptor of arealization. (a) The three global connectopies were plotted together in what we termed the global connectopic space, with connectopy values assigned to the RGB values at each vertex. The global connectopic space integrates the information of three global connectopies and quantifies the topography of the dominant global connectopy. **(b)** Left: Several lobes or subregions clearly appear when every two global connectopies are plotted together on the 2D space, with the extremes of GCs clearly and continuously shown. GC1-DV and GC2-RC split the cortex into the prefrontal cortex and limbic cortex, sensorimotor and motor cortex, and occipitotemporal cortex. GC1-DV and GC3-ML split the cortex into the frontal cortex, limbic cortex, and occipitotemporal cortex. GC2-RC and GC3-ML split the cortex into the prefrontal cortex, limbic cortex, and other regions. Right: The three GCs were plotted together in the 3D space. Vertices were assigned different colors according to the signs of the three axes. **(c)** Modules identified by hierarchical clustering using the three global connectopies. At each level, the brain was partitioned into two modules according to the positive and negative signs of the global connectopy. Eight modules, including lobes or functional networks, emerged clearly. vSomaMot ventral somatomotor cortex, dSomaMot dorsal somatomotor cortex, lPFC lateral prefrontal cortex, CG cingulate gyrus, lTC lateral temporal cortex, AG angular gyrus, mOC medial occipital cortex, OPC occipital polar cortex, OFC orbitofrontal cortex, vmPFC ventromedial prefrontal cortex, PCC posterior cingulate cortex.

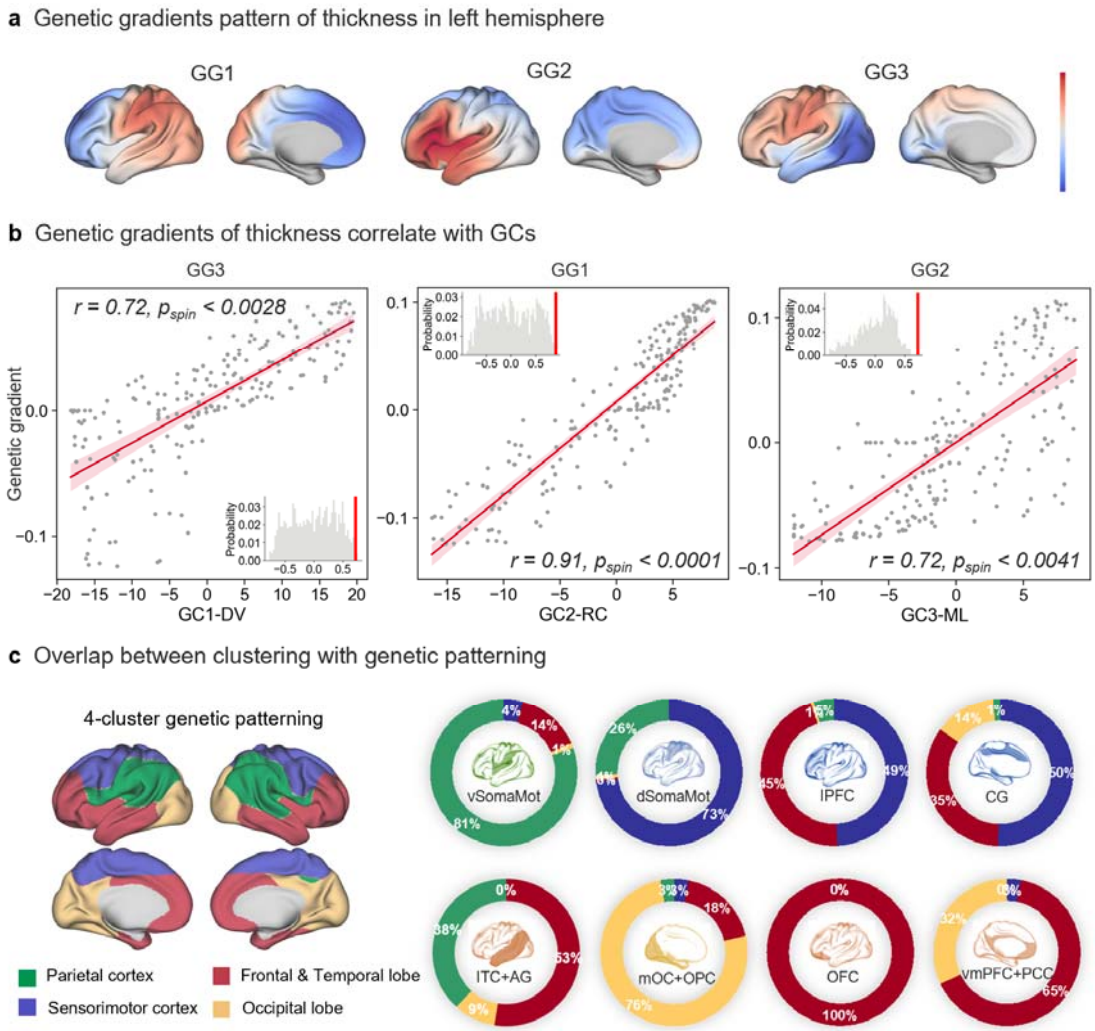

Figure 4. Global connectopies correspond to genetic topography. (a) The first three gradients of genetic similarity of cortical thickness. The genetic similarity matrix was calculated by fitting bivariate ACE models to compute the genetic correlations of the cortical thickness between two vertices in a twin dataset. **(b)** The three gradients of genetic similarity of cortical thickness show a high correlation with global connectopies ($r_{\text{GC1-DV, GG3-Thickness}} = 0.72$, $p_{\text{spin}} < .0028$, FDR corrected; $r_{\text{GC2-RC, GG1-Thickness}} = 0.91$, $p_{\text{spin}} < .0001$, FDR corrected; $r_{\text{GC3-ML, GG2-Thickness}} = 0.72$, $p_{\text{spin}} < .0041$, FDR corrected). **(c)** Overlap between four modules derived from hierarchical clustering with genetic patterning of cortical thickness. Four-cluster genetic patterning was obtained by performing fuzzy clustering on the genetic similarity matrix, which corresponds to well-known brain regions. *** $p < .001$, ** $p < .01$, * $p < .05$.

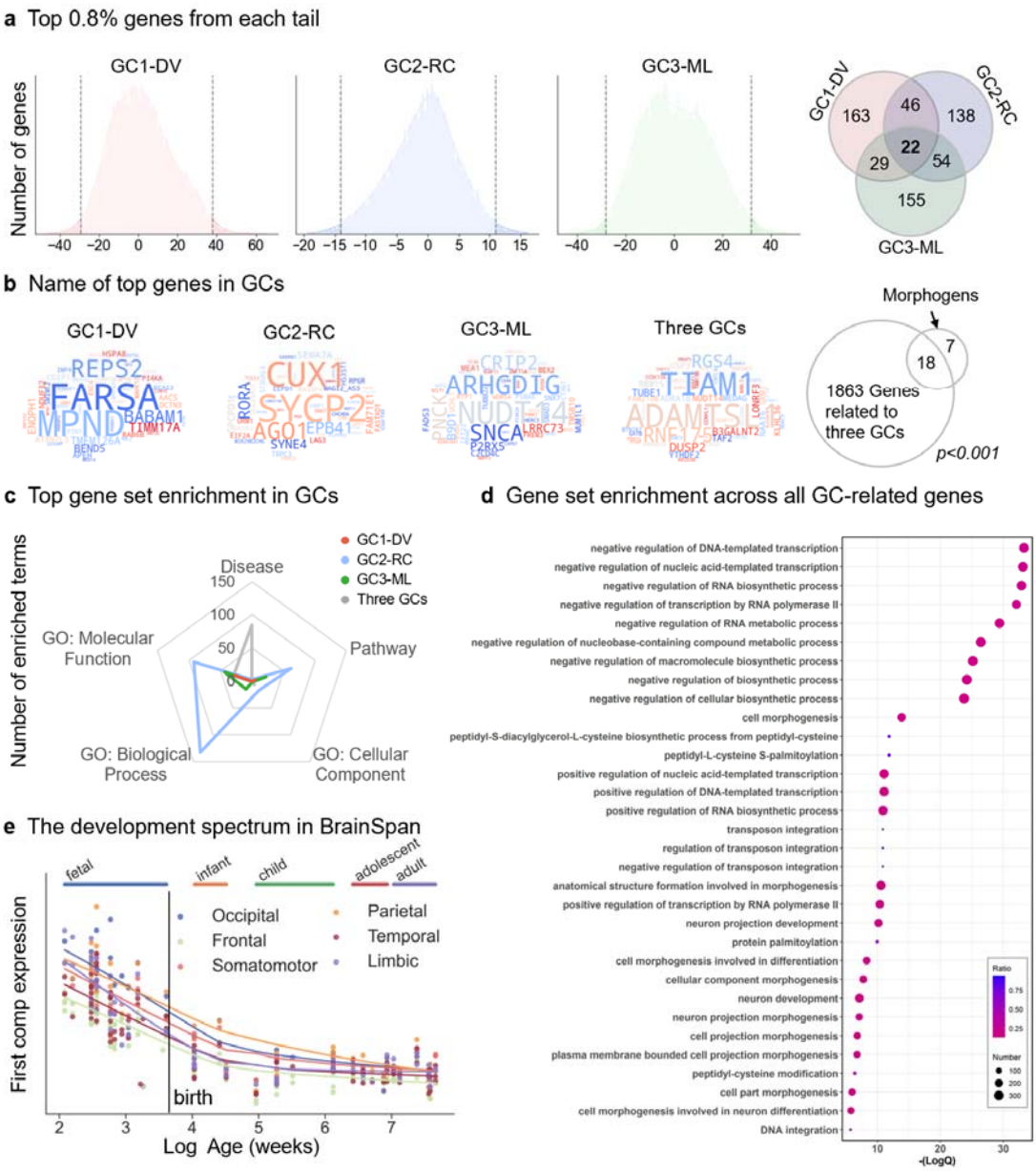

Figure 5. Gene enrichment analysis of connectopy-associated genes. (a) Distributions of connectopic weights across genes. Genes in the top 0.8% of either tail of the distribution (n = 130) were selected for further enrichment analysis. The Venn diagram showing the overlap of genes is shown on the right. **(b)** Top genes for unique connectopy and overlap of connectopies. **(c)** Gene set enrichment was conducted on genes belonging to each global connectopy and all three connectopies. **(d)** Gene set enrichment across all global connectopy-related genes indicated terms related to the regulation of transcription, metabolic process, morphogenesis, cellular development, and neuron projection. **(e)** The development spectrum of gene expression for each brain macrostructure. Genes associated with global connectopies were expressed highly in the prenatal period and decreased after birth.

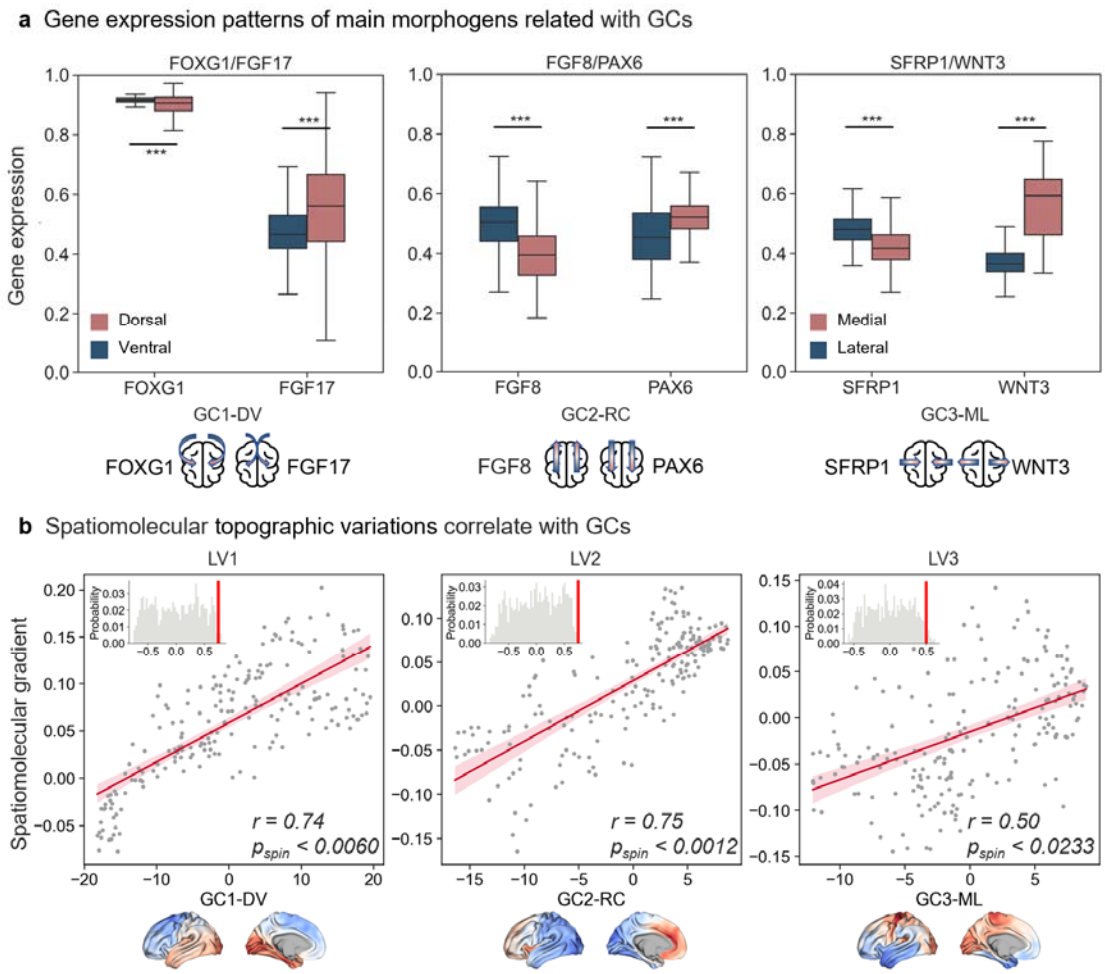

Figure 6. Potential genetic basis underlying global connectopies. (a) The expression of genes that express the same pattern as any of the three global connectopies was significantly different between the two ends of the global connectopies (two-sample t-test, all $p < .001$). **(b)** The global connectopies significantly correlated with the spatiomolecular gradients, which maintained the same pattern as morphogenetic gradients during development ($r_{\text{GC1-DV, LV1}} = 0.74$, $p_{\text{spin}} < .0060$, FDR corrected; $r_{\text{GC2-RC, LV2}} = 0.75$, $p_{\text{spin}} < .0012$, FDR corrected; $r_{\text{GC3-ML, LV3}} = 0.5$, $p_{\text{spin}} < .0233$, FDR corrected). *** $p < .001$.

Figures and Tables

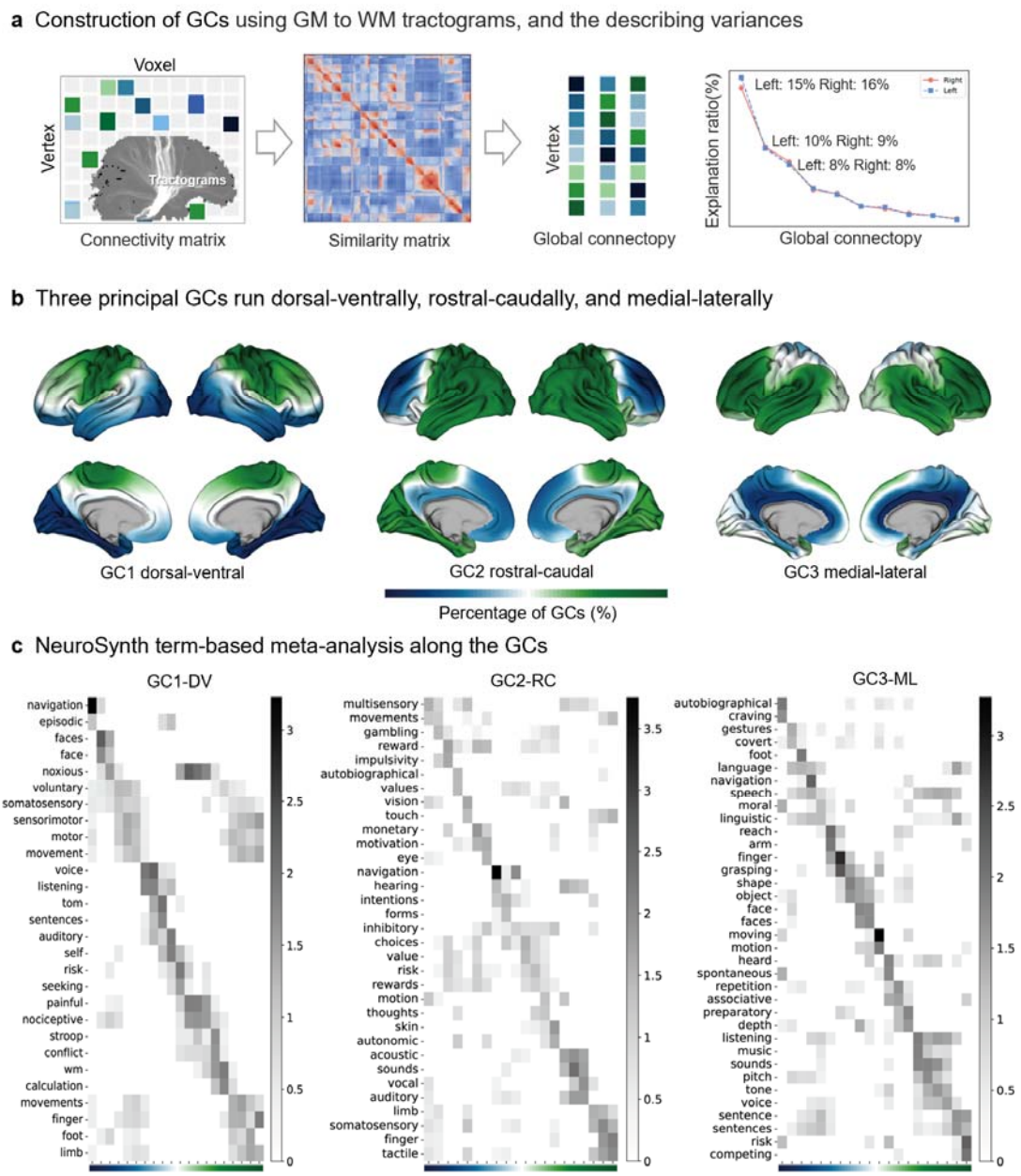

Figure 1. Three global connectopies in the human cerebral cortex. (a) The construction of global connectopies. White matter tractograms were calculated to get a similarity matrix, i.e., a tractogram covariance (TC) matrix. Diffusion embedding was implemented on the TC matrix, resulting in low-dimensional gradients. A scree plot describing variance is shown on the right. **(b)** The first three global connectopies ran dorsoventrally, rostrocaudally, and mediolaterally and were termed GC1-DV, GC2-RC, and GC3-ML, respectively. **(c)** NeuroSynth term-based meta-analysis along the global connectopies. Terms that had the highest two z-scores for each binarized mask of the global connectopies were included in this visualization.

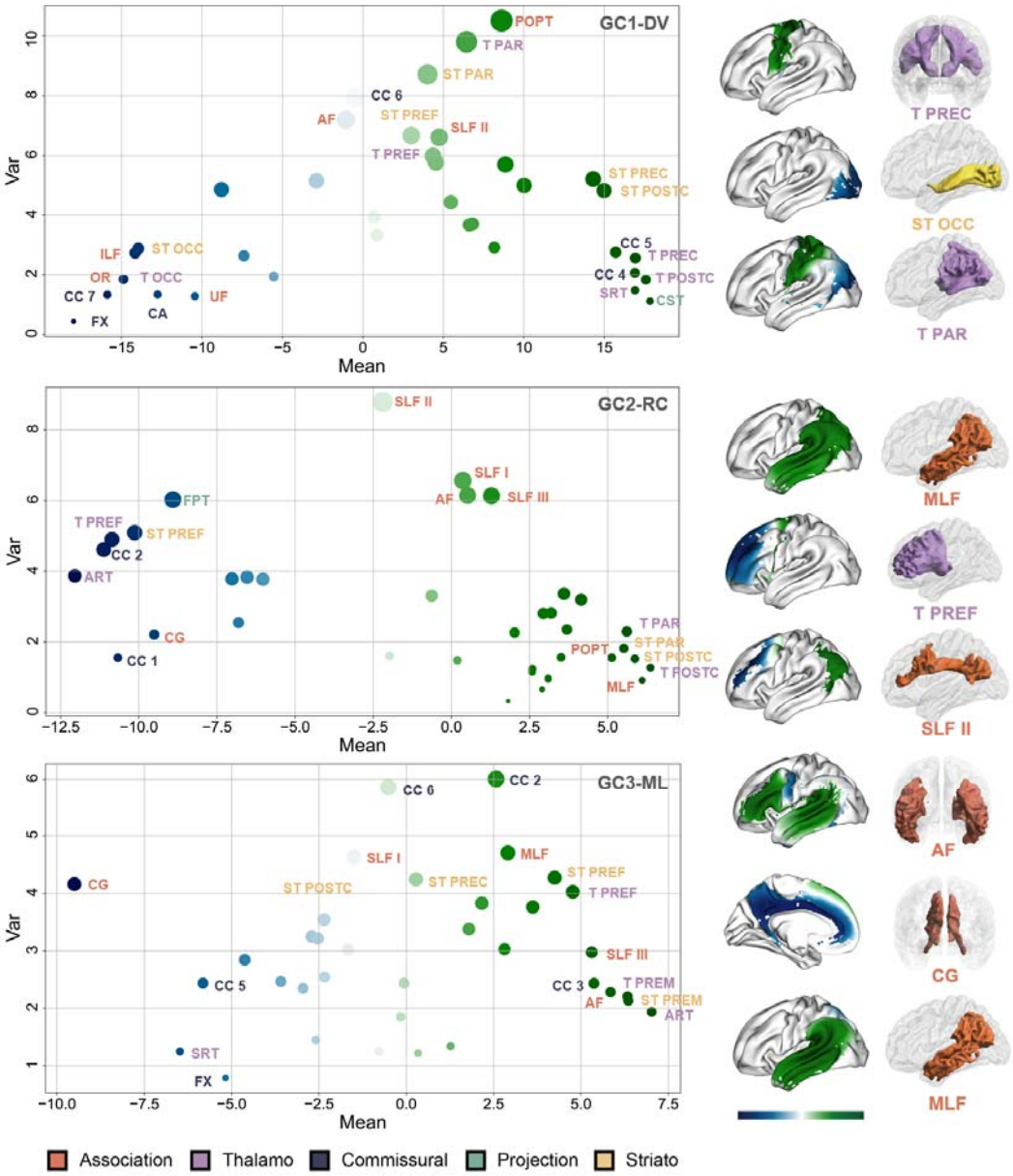

Figure 2. The three global connectopies are situated by distinct sets of white matter tracts. Mean values and variances of the contribution of five types of tracts to the global connectopies are shown. Each dot represents one tract. Different colors represented different types of tracts, with deeper colors for higher contributions. The right two columns show two types of characteristic tracts contributing to the global connectopies, with one type of tract situated at one extreme of the global connectopy and the other stretched across the global connectopy. The first column shows the cortical projection on the surface of the tract, and the second shows the corresponding fiber bundles reconstructed by TractSeg.

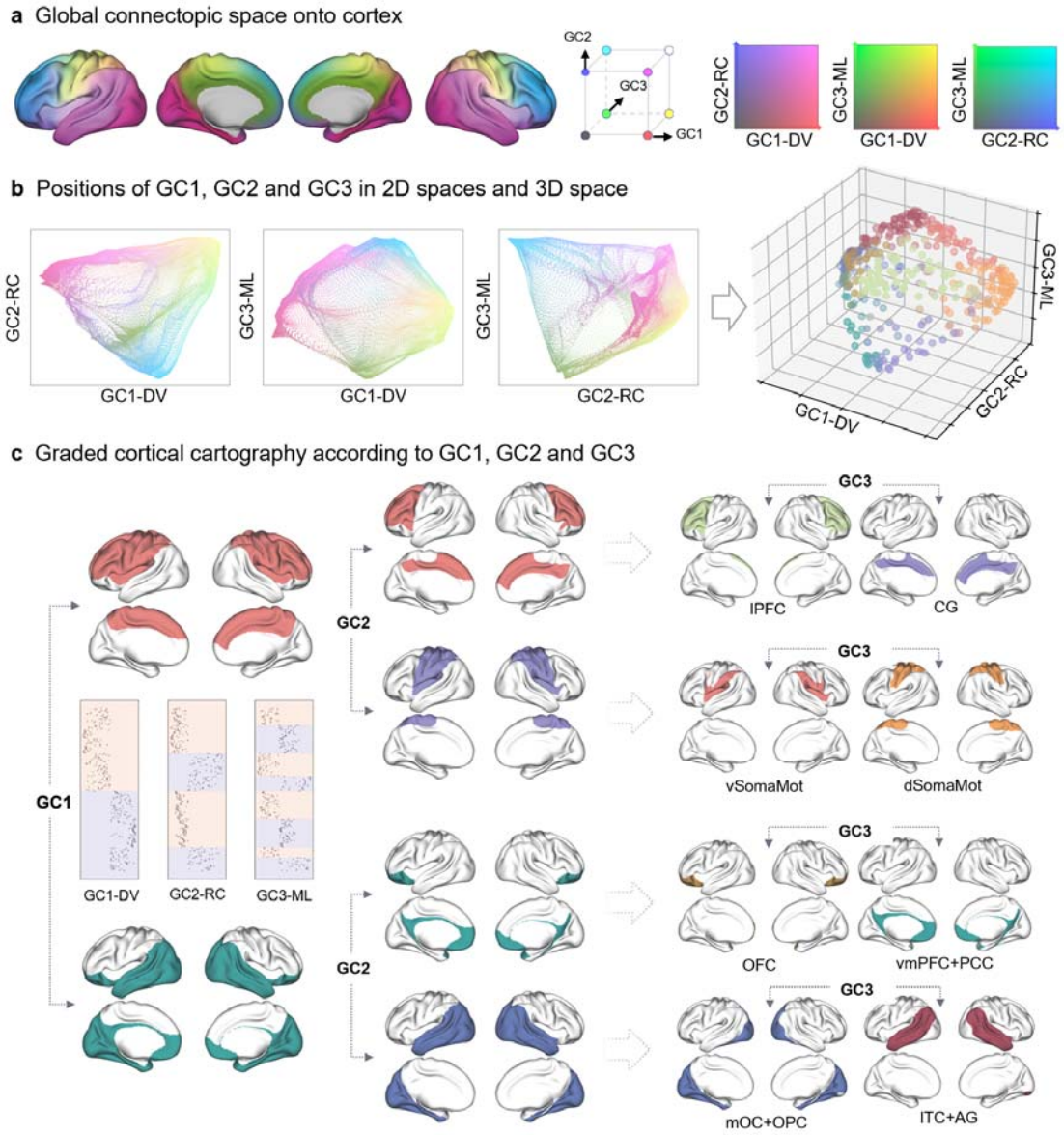

Figure 3. Global connectopies provide a large-scale descriptor of arealization. (a) The three global connectopies were plotted together in what we termed the global connectopic space, with connectopy values assigned to the RGB values at each vertex. The global connectopic space integrates the information of three global connectopies and quantifies the topography of the dominant global connectopy. **(b)** Left: Several lobes or subregions clearly appear when every two global connectopies are plotted together on the 2D space, with the extremes of GCs clearly and continuously shown. GC1-DV and GC2-RC split the cortex into the prefrontal cortex and limbic cortex, sensorimotor and motor cortex, and occipitotemporal cortex. GC1-DV and GC3-ML split the cortex into the frontal cortex, limbic cortex, and occipitotemporal cortex. GC2-RC and GC3-ML split the cortex into the prefrontal cortex, limbic cortex, and other regions. Right: The three GCs were plotted together in the 3D space. Vertices were assigned different colors according to the signs of the three axes. **(c)** Modules identified by hierarchical clustering using the three global connectopies. At each level, the brain was partitioned into two modules according to the positive and negative signs of the global connectopy. Eight modules, including lobes or functional networks, emerged clearly. vSomaMot ventral somatomotor cortex, dSomaMot dorsal somatomotor cortex, lPFC lateral prefrontal cortex, CG cingulate gyrus, lTC lateral temporal cortex, AG angular gyrus, mOC medial occipital cortex, OPC occipital polar cortex, OFC orbitofrontal cortex, vmPFC ventromedial prefrontal cortex, PCC posterior cingulate cortex.

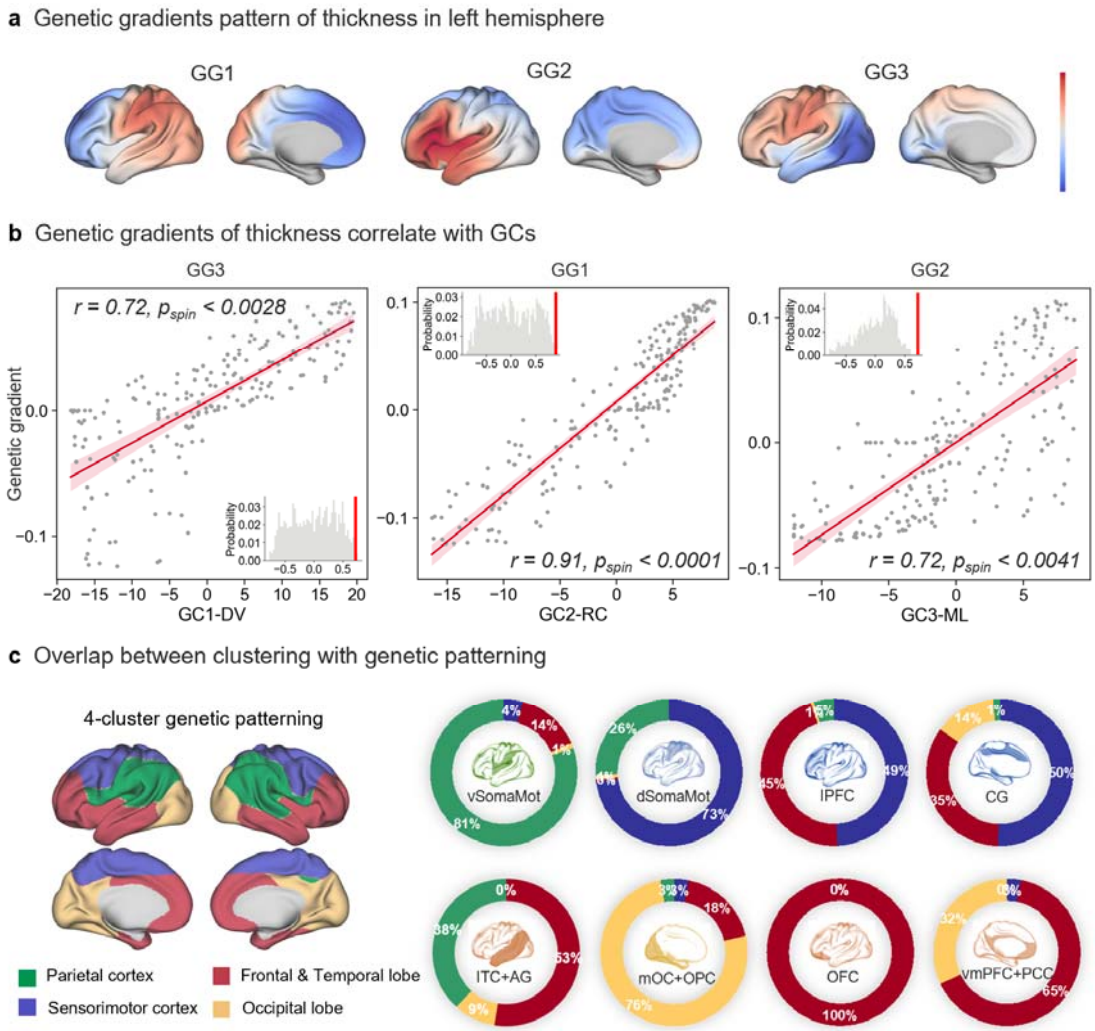

Figure 4. Global connectopies correspond to genetic topography. (a) The first three gradients of genetic similarity of cortical thickness. The genetic similarity matrix was calculated by fitting bivariate ACE models to compute the genetic correlations of the cortical thickness between two vertices in a twin dataset. **(b)** The three gradients of genetic similarity of cortical thickness show a high correlation with global connectopies ($r_{\text{GC1-DV, GG3-Thickness}} = 0.72$, $p_{\text{spin}} < .0028$, FDR corrected; $r_{\text{GC2-RC, GG1-Thickness}} = 0.91$, $p_{\text{spin}} < .0001$, FDR corrected; $r_{\text{GC3-ML, GG2-Thickness}} = 0.72$, $p_{\text{spin}} < .0041$, FDR corrected). **(c)** Overlap between four modules derived from hierarchical clustering with genetic patterning of cortical thickness. Four-cluster genetic patterning was obtained by performing fuzzy clustering on the genetic similarity matrix, which corresponds to well-known brain regions. *** $p < .001$, ** $p < .01$, * $p < .05$.

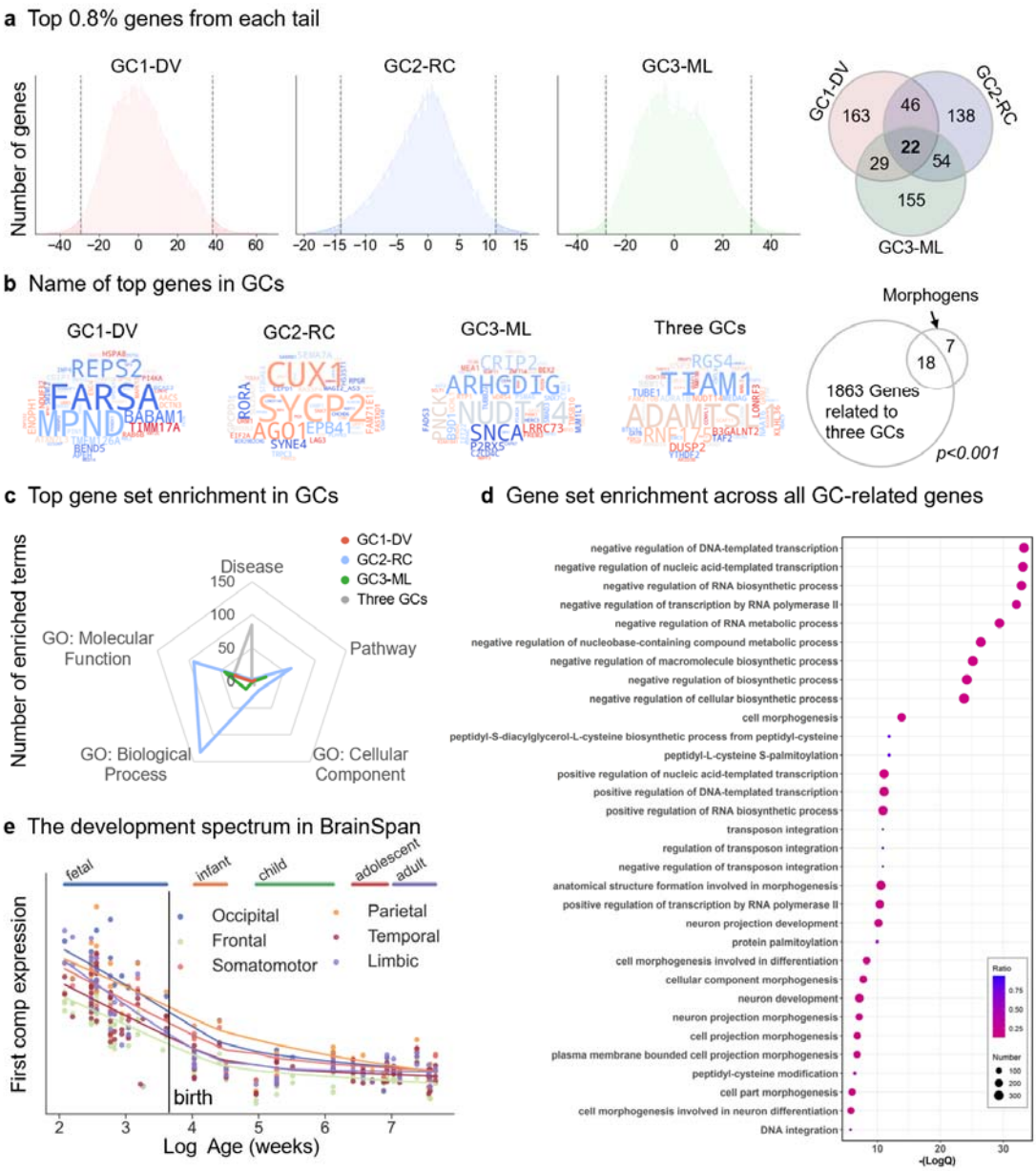

Figure 5. Gene enrichment analysis of connectopy-associated genes. (a) Distributions of connectopic weights across genes. Genes in the top 0.8% of either tail of the distribution (n = 130) were selected for further enrichment analysis. The Venn diagram showing the overlap of genes is shown on the right. **(b)** Top genes for unique connectopy and overlap of connectopies. **(c)** Gene set enrichment was conducted on genes belonging to each global connectopy and all three connectopies. **(d)** Gene set enrichment across all global connectopy-related genes indicated terms related to the regulation of transcription, metabolic process, morphogenesis, cellular development, and neuron projection. **(e)** The development spectrum of gene expression for each brain macrostructure. Genes associated with global connectopies were expressed highly in the prenatal period and decreased after birth.

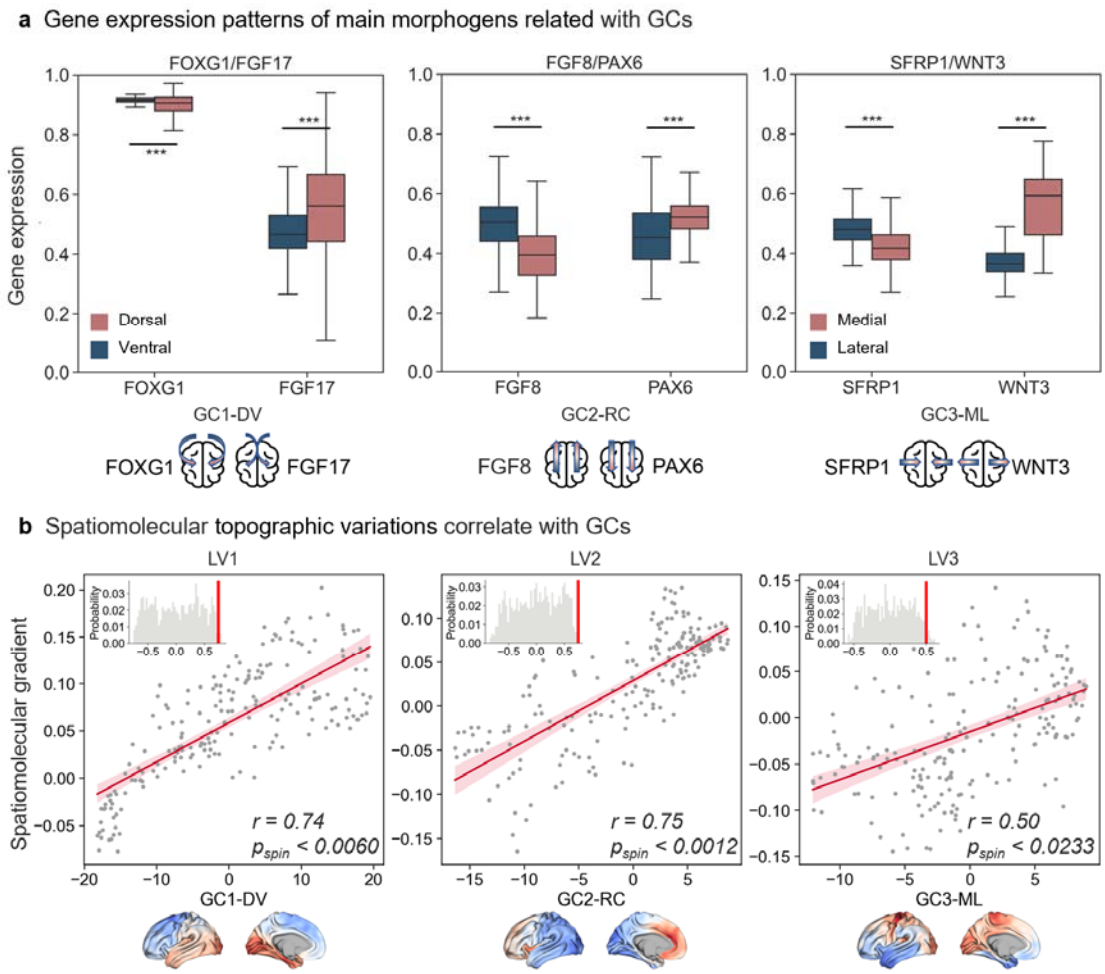

Figure 6. Potential genetic basis underlying global connectopies. (a) The expression of genes that express the same pattern as any of the three global connectopies was significantly different between the two ends of the global connectopies (two-sample t-test, all $p < .001$). **(b)** The global connectopies significantly correlated with the spatiomolecular gradients, which maintained the same pattern as morphogenetic gradients during development ($r_{\text{GC1-DV, LV1}} = 0.74$, $p_{\text{spin}} < .0060$, FDR corrected; $r_{\text{GC2-RC, LV2}} = 0.75$, $p_{\text{spin}} < .0012$, FDR corrected; $r_{\text{GC3-ML, LV3}} = 0.5$, $p_{\text{spin}} < .0233$, FDR corrected). *** $p < .001$.